# Paleomagnetic and structural constraints on the Neogene evolution of the Soma basin as part of the İzmir–Balıkesir Transfer Zone (western Anatolia)

MSc-thesis Jan Westerweel, Utrecht University

*Fieldwork in the Soma basin, western Anatolia*

## Information

Studentnumber: *3795748*
Contact: *j.westerweel@students.uu.nl*
Department: *Paleomagnetic lab "Fort Hoofddijk" Faculty of Earth Sciences, Utrecht University*
Supervised by: *prof. dr. C.G. Langereis (Utrecht University) & dr. B. Uzel (Dokuz Eylül University)*
Credits: *45 ECTS*
First version received: 31-10-2016
Final version received: 14-12-2016
Keywords: *paleomagnetism, vertical-axis rotation, Neogene, Soma basin, İzmir-Balıkesir Transfer Zone, strike-slip faulting, transtension, western Anatolia, Aegean tectonics, back-arc extension, Turkey*

# Abstract

The İzmir–Balıkesir Transfer Zone (İBTZ) is a major tectonic feature in western Anatolia since the Neogene, because it accommodates differential extension between the large-scale Menderes (MCC) and Cycladic (CCC) core complexes. However, there is still much discussion whether this extension occurred in a single or in multiple deformation phases. Furthermore, the northern continuation of the İBTZ remains relatively unstudied in this aspect. This part is especially crucial in obtaining a complete picture of the western Anatolian tectonic history, as there could be a relationship between the İBTZ and the North Anatolian Fault Zone (NAFZ).
The goal of this study is therefore to constrain the deformation history of the Soma basin, located in the northern part of the İBTZ. To this end, new paleomagnetic, structural and stratigraphic data were acquired there.
The new data indicates that the Soma basin evolved as a pull-apart basin as part of the İBTZ during at least two transtensional deformation phases. During the first Early-Middle Miocene phase, deformation was characterized by NE-SW trending dextral strike-slip faulting and rigid-block rotations of on average 29 ± 8° clockwise. This indicates that the İBTZ evolved as a wide dextral shear zone during the first phase, accommodating asymmetric extensional exhumation of the MCC and a differential amount of extension in the CCC. During the second Late Miocene-Pliocene deformation phase, the mode of extension in the Aegean region switched from localized to distributed, related to slab-tearing of the Aegean slab and subsequent acceleration of rollback. In the Soma basin, this is evidenced by a narrowing of the İBTZ, resulting in decoupling of NE-SW trending dextral strike-slip faulting and E-W trending normal faulting. In this context, only the northern part of the Soma basin could have been influenced by the NAFZ, because more intense deformation and incoherent rotations were found there.

# Table of Contents

# 1. Introduction

Western Anatolia is one of the hot topics in geoscience research, mainly due to its complex deformation history. The region is dominated by NNE trending extensional deformation since the Middle Eocene in the African-European convergent tectonic setting. There are currently two major hypotheses for the cause of this extension. One hypothesis is the westward escape of Anatolia *(Dewey et al., 1986; Şengör, 1979; Şengör & Yılmaz, 1981; Şengör et al., 1985)*. This process could have led to the formation of the dextral North Anatolian Fault Zone (NAFZ), as well as of the sinistral East Anatolian Fault Zone (EAFZ). The second hypothesis is related to slab rollback of the Aegean slab and consequent back-arc extension *(Biryol et al., 2011; Le Pichon & Angelier, 1979; Meulenkamp et al., 1988; van Hinsbergen et al., 2005b, 2010)*. Several studies have combined these two hypotheses, suggesting that rollback of the Aegean slab could have been a cause for the westward escape of Anatolia *(Bozkurt, 2001; Brun et al., 2016)*.
In any case, Cenozoic extension in western Anatolia has resulted in two regional extensional features, namely the Cycladic (CCC) and Menderes (MCC) metamorphic core complexes. Moreover, recent studies have constrained another tectonic feature which is located between the MCC and CCC and south of the NAFZ. The İzmir-Balıkesir Transfer Zone (İBTZ) was first identified by Okay and Siyako *(1993)*, who suggested that this NE-SW trending zone was the depositional loci of the Bornova Flysch Zone, a regional olistostrome–mélange belt, during the Late Cretaceous *(Erdoğan, 1990; Okay et al., 2012; Sarı, 2012)*. However, more recent studies suggest that it is a NE-SW trending shear zone *(Morris & Anderson 1996; Pe-Piper et al., 2002; Philippon et al., 2012, 2014; Ring et al., 1999; Sözbilir et al., 2003; Uzel & Sözbilir, 2008; Walcott & White 1998; Uzel et al., 2013, 2015)*. These studies argue that transtensional deformation within this fault zone accommodates differential extensional strain between the CCC and MCC since the Miocene, alongside the Mid-Cycladic Lineament (MCL). This is another NE-SW trending fault zone located to the southwest of the İBTZ. Pre-Neogene basement rocks, Miocene volcano-sedimentary units and Quaternary continental units were all deposited and deformed within the İBTZ *(Kaya, 1981; Sözbilir et al., 2011; Uzel and Sözbilir, 2008; Uzel et al., 2012, 2013)*. In addition, Gessner et al. *(2013)* and Uzel et al. *(2015)* suggested that the İBTZ is a surface expression of a subduction transform edge propagator fault (STEP-fault) related to slab-tearing of the Aegean slab due to rollback (*Govers & Wortel, 2005)*. Figure 1 shows a schematic overview of this process. Several studies *(Brun et al., 2016; Uzel et al., 2015)* suggested a connection between this slab rollback, the İBTZ and the NAFZ. For these reasons, understanding the northern continuation of the İBTZ and its relationship with the NAFZ could lead to a more complete picture of western Anatolian tectonics.
However, there is another crucial uncertainty in constraining the tectonic history of western Anatolia. Several studies suggest that the Cenozoic extension took place in a single deformation phase *(Glodny & Hetzel, 2007; Seyitoğlu et al., 2000, 2002, 2004; van Hinsbergen et al., 2010)*, while others suggest that it occurred during multiple deformation phases separated by periods of inversion and tectonic quiescence (*Beccaletto & Steiner, 2005; Bozkurt, 2001; Bozkurt & Sözbilir, 2004, 2006; Bozkurt & Mittwede, 2005; Emre & Sözbilir 2007; Kaya et al., 2004, 2007; Kaymakcı 2006; Koçyiğit et al., 1999; Purvis & Robertson 2004, 2005; Sözbilir, 2001; Yılmaz et al., 2000)*. The role and evolution of the İBTZ within this tectonic setting are not well-understood either. One possible reason for this is that past paleomagnetic studies in the Aegean region were mainly concerned with the NAFZ, western and central Turkey and Greece.

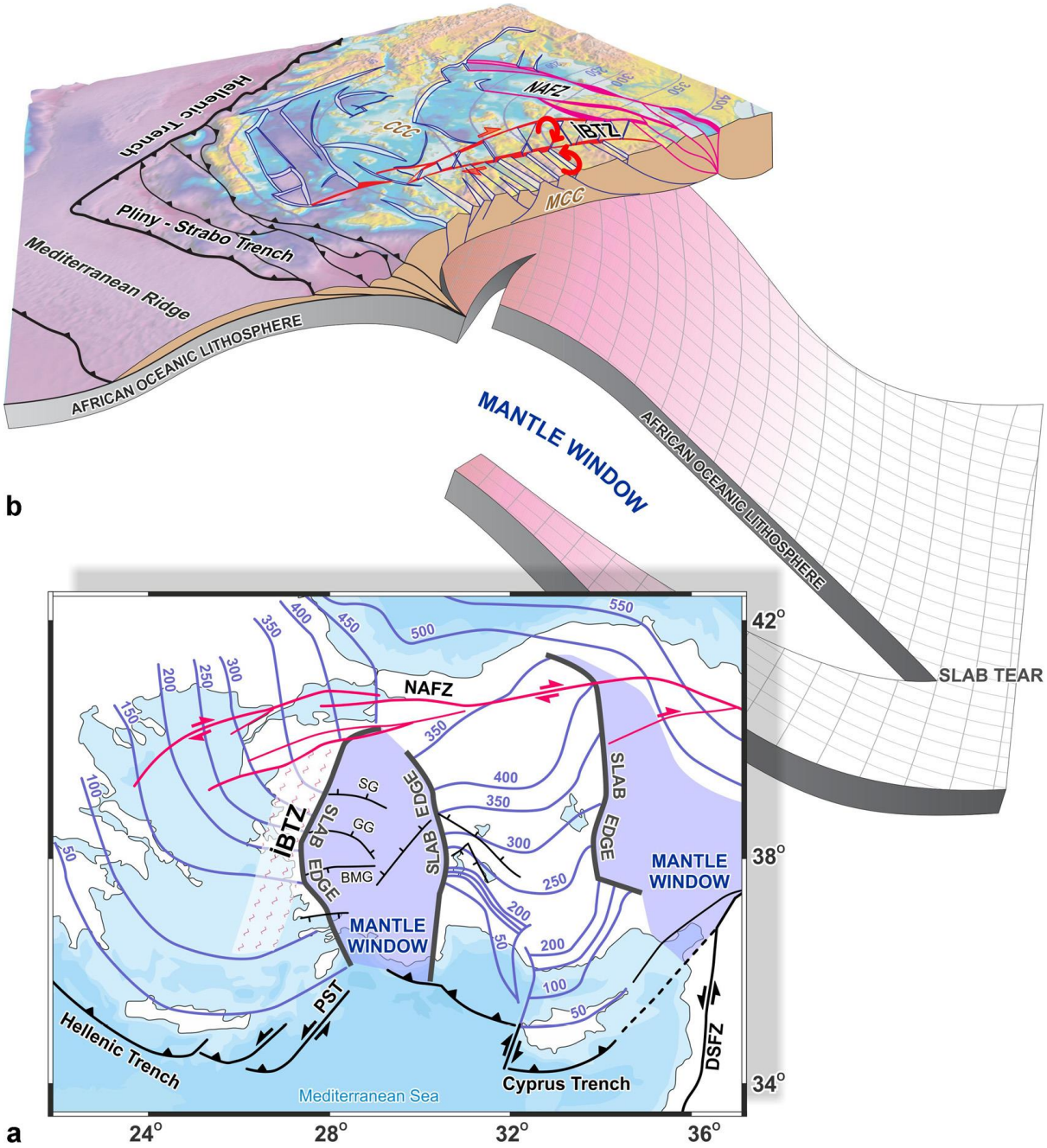


*Fig. 1: a) Schematic map highlighting the main tectonic features of the Aegean and western Anatolian region (after Biryol et al., 2011). Abbreviations: İBTZ = İzmir–Balıkesir Transfer Zone, MCC = Menderes Core Complex, CCC = Cycladic Core Complex, NAFZ = North-Anatolian Fault Zone. The presumed mantle window related to slab-tearing is indicated east of the İBTZ; b) Schematic surface to mantle 3D-model depicting the slab-tear in the Aegean slab alongside the İBTZ, MCC and CCC (after Uzel et al., 2015). Vertical-axis rotations as constrained by paleomagnetism are shown in red. Abbreviations: DSFZ = Dead Sea Fault Zone, PST = Pliny-Strabo Trench, SG = Simav Graben, GG = Gediz Graben, BMG = Büyük Menderes Graben*

To this end, Uzel & Sozbilir *(2008)* and Uzel et al. *(2013, 2015, 2016)* conducted structural and paleomagnetic research within the southern part of the İBTZ and adjacent regions (Fig. 2). These investigations showed that multiple strike-slip dominated deformation phases

occurred throughout the İBTZ during the Neogene. According to the structural data, at least three deformation phases took place *(Uzel & Sozbilir, 2008; Uzel et al., 2013).*

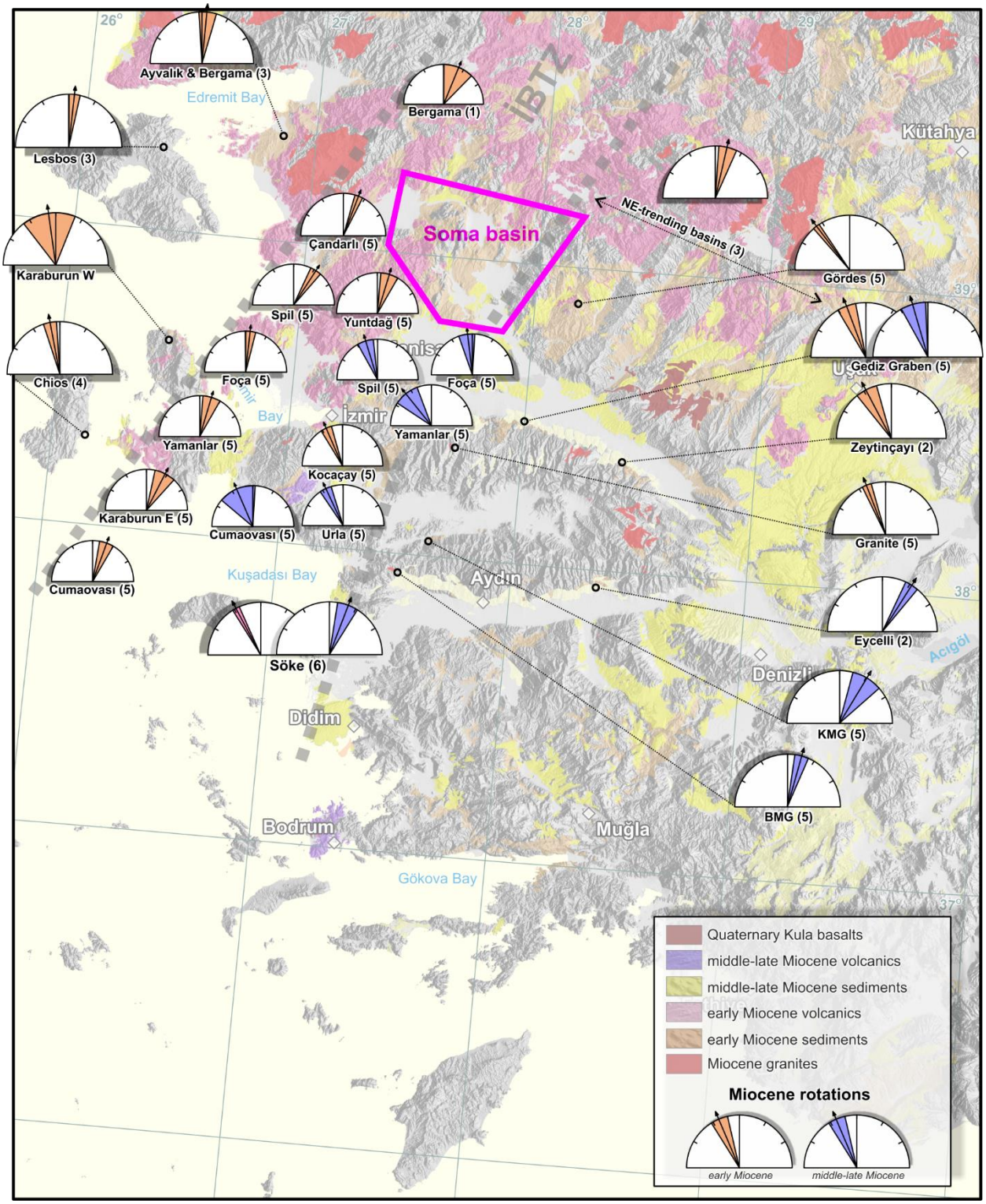


*Fig. 2: Miocene paleomagnetic results in western Anatolia from previous studies. Numbers refer to (1) Kissel et al. (1987), (2) Şen and Seyitoğlu (2009), (3) van Hinsbergen et al. (2010), (4) Kaymakci et al. (2007), (5) Uzel et al. (2015), (6) Uzel et al. (2016). The Soma basin (study area of this research) is indicated as well (after Uzel et al., 2016). Abbreviations: İBTZ = İzmir–Balıkesir Transfer Zone, KMG = Küçük Menderes Graben, BMG = Büyük Menderes Graben*

The paleomagnetic data constrained at least two relatively homogeneous rotational phases *(Uzel et al., 2015)*. These two rotational phases are separated by a Middle Miocene angular unconformity *(Uzel et al., 2016)*. Deformation and rotation within the İBTZ were relatively different compared to adjacent regions. This indicates that the İBTZ evolved as a system of rigid-body rotation related to orthogonal extension *(Jolivet & Brun, 2010; Uzel et al., 2015).* These observations do not completely agree with the conclusions of van Hinsbergen et al. *(2010)*, who did not recognize the occurrence of rigid-block rotations within parts of the İBTZ and only distinguished one Miocene rotational phase in western Anatolia, related to asymmetrical exhumation of the MCC. Furthermore, these observations directly oppose the ideas of Kondopoulou et al. *(2011)*, who proposed that western Anatolia is a region of chaotic rotations.
The logical next step is to investigate the northern continuation of the İBTZ system in this context. This could provide crucial insight in the suggested connection between the İBTZ and the NAFZ. Furthermore, new data could provide insight in the relationship between the multiple-phase formation of the İBTZ from Uzel et al. *(2013, 2015, 2016)* and the single-phase asymmetrical exhumation of the MCC from van Hinsbergen et al. *(2010)*. Therefore, the goal of this research is to constrain the Neogene deformation history of the Soma basin, western Anatolia, and adjacent regions (Fig. 2). This area is located at a cross-point directly north of the studied part of the İBTZ by Uzel et al. *(2013, 2015, 2016)*, directly west of the study area from van Hinsbergen et al. *(2010)* and proximal to the southern strands of the NAFZ. To this end, new paleomagnetic data will be acquired there, as well as new structural, stratigraphic and Anisotropy of Magnetic Susceptibility (AMS) data.

# 2. Geological setting

Western Anatolia is a region with a complex deformation history, where NNE trending extension and exhumation has taken place since the Middle Eocene after an Alpine active margin phase *(Bozkurt, 2001; Şengör et al., 1985; Uzel et al., 2013)*. Figure 3 shows a general geological map of western Anatolia alongside the larger-scale tectonic setting of African-European convergence. The main geological features of the region are the Menderes Core Complex (MCC), the Cycladic Core Complex (CCC) and the NE-SW trending İzmir-Balıkesir Transfer Zone (İBTZ). The Soma basin is one of the basins located within the İBTZ. All these features will be described below in more detail.

## 2.1. The Menderes Core Complex

The geology of the Menderes region, directly east of the İBTZ, is characterized by the MCC which is cross-cut by NE-SW trending Late Cenozoic basins in the northern part. These basins are hence called the Northern Menderes Massif basins (NMM-basins). The largest of these are from west to east the Gördes, Demirci, Selendi and Uşak-Güre basins *(Şengor, 1987; van Hinsbergen et al., 2010)*. The basins are bounded on their northern and southern margins by E-W trending detachment faults as well as high angle normal faults. On their eastern and western margins, the basins are bounded by dextral or sinistral strike-slip faults which were interpreted by Şengör *(1987)* as cross-faults related to differential extension.

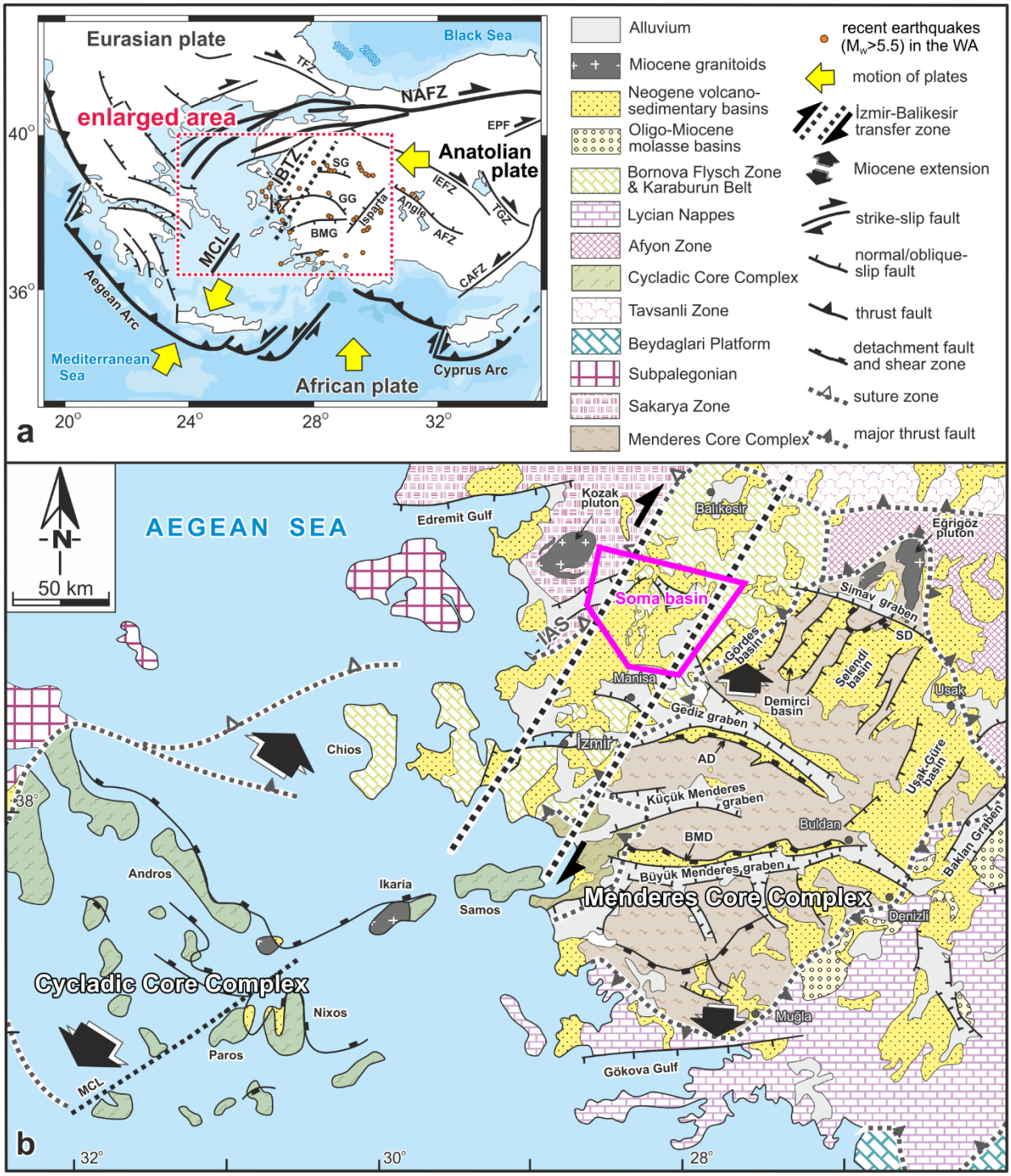


*Fig. 3: a) Large-scale tectonic setting of the Aegean region with its main features. The Soma basin is indicated as well (after Kaymakci et al., 2007; Koçyiğit and Özaçar, 2003; Taymaz et al., 2007; Uzel et al., 2013). Abbreviations: NAFZ = North Anatolian fault zone, İBTZ = İzmir–Balıkesir Transfer Zone, MCL= Mid-Cycladic Lineament, NAFZ = North-Anatolian Fault Zone, CAFZ = Central Anatolian fault zone, EPF = Ezinepazarı Fault, TGZ = Tuz Gölü Fault Zone, İEFZ = İnönü-Eskişehir fault zone, AFZ = Akşehir fault zone, BMG = Büyük Menderes Graben, GG = Gediz Graben, SG = Simav Graben, TFZ = Thrace fault zone; b) General geological map of western Anatolia with the main tectonic features and Cenozoic successions indicated: AD = Alaşehir Detachment Fault, BMD = Büyük Menderes Detachment Fault, SD = Simav detachment, İAS = İzmir–Ankara Suture*

Therefore, most of these basins have been interpreted as upper crustal supradetachment basins related to rapid, NNE-SSW trending extension of young, hot crust, resulting in domal uplift and exhumation of the crustal-scale MCC during the Oligocene-Miocene *(Bozkurt, 2000; Bozkurt & Sözbilir, 2006; Çiftçi & Bozkurt, 2009; Koçyiğit et al., 1999; Sözbilir, 2001, 2002).* According to van Hinsbergen et al. *(2010),* this exhumation occurred asymmetrically with the Büyük Menderes (BMD) and Alaşehir (AD) detachments defining a pivot point, separating clockwise (CW) rotation in the north and counter-clockwise (CCW) in the south. The stratigraphy of the MCC consists of two sequences: a high-grade metamorphic core which consists of augen gneisses, metagranites, schists, paragneisses and metagabbros and a lower-grade metamorphic cover which consists of schists, quartzites, amphibolites, phyllites and marbles. Its metamorphic history can be traced back to Late Proterozoic to Early Paleozoic Pan-African events as well as to Mesozoic to Cenozoic Alpine orogenic events *(Akkök, 1983; Bozkurt & Park, 1997; Candan et al., 1997, 2001; Okay, 2001).*

## 2.2. The Cycladic Core Complex

The CCC and related detachment faulting is less exposed in western Anatolia compared to the Menderes region. It is mainly exposed in the southern margin of the Turkish Kocaçay Basin and in a crescent-shape belt composed of several Greek islands. The main event that influenced the CCC is Aegean subduction during the Eocene, hence the metamorphism is high-pressure in nature. At some places, high-temperature metamorphism is superimposed on the high-pressure metamorphism *(Brun et al., 2016; Philippon et al. 2012).* The main rocks that comprise the CCC are mica- and calc-schists, marbles, meta-cherts, serpentines and meta-volcanic rocks *(Okay, 2001; Sözbilir et al., 2011).* Like the MCC, exhumation in the CCC took place during the Oligocene-Miocene *(Vandenberg & Lister, 1996).* It is cross-cut by basins with a progressively more continental sedimentary infill of similar age separated by large-scale detachments, comparable to the MCC *(Brun et al, 2016).*

## 2.3. The İBTZ

The İBTZ itself is recognized by most studies as a NE-SW trending transtensional shear zone, accommodating differential extension between the MCC and CCC *(Ring et al., 1999; Uzel & Sözbilir, 2008; Sözbilir et al., 2011; Uzel et al., 2013, 2015).* It is dominated by dextral strike-slip deformation from the Miocene until recent, as evidenced by GPS data and earthquake focal mechanisms *(Aktuğ & Kılıçoğlu, 2006; İnan et al., 2012; Uzel et al., 2013; Zhu et al., 2006).* It has been suggested that the İBTZ is a surface expression of a slab-tear induced by rollback of the Aegean slab. This slab-tear forms a lateral boundary of the Hellenic trench system (Fig 1). Mantle windows often coincide with the location of the slab edge that forms during the formation of a slab-tear *(Biryol et al., 2011; Govers & Wortel, 2005; Jolivet et al., 2013; van Hinsbergen et al., 2010).* According to results from tomography *(Biryol et al., 2011; Paul et al., 2014; van Hinsbergen et al, 2010),* surface observations *(Gessner et al., 2013; Ring et al., 1999; Uzel et al., 2013, 2015)* and geochemistry *(Aldanmaz et al., 2000; Altunkaynak et al., 2010; Genç et al., 2001; Pe-Piper et al., 2002),* there is indeed evidence for such a mantle window (Fig. 1), adding further credibility to the hypothesis that the İBTZ is a surface expression of a slab-tear.
The formation of the İBTZ was accompanied by volcanism *(Genç et al., 2001; Uzel & Sözbilir, 2008; Sözbilir et al., 2011).* Previous studies constrained at least three deformation phases *(Uzel et al., 2013)* and two rotational phases *(Uzel et al., 2015, 2016)* within the İBTZ. The first deformation phase was dominated by NE-SW trending transtension during the Early

to Late Miocene. This led to the formation of NE-SW trending basins within the zone. It has been suggested that these basins follow older structural trends *(Kaya, 1981).* The first deformation phase was followed by a second during the Pliocene which was characterized by overall pure strike-slip deformation. Moreover, the second deformation phase coincided with the final exhumation phase of the MCC, the development of the North Anatolian Fault Zone (NAFZ) and the last activity of the Mid-Cycladic Lineament (MCL). During the third deformation phase in the Late Pliocene-Quaternary, the İBTZ evolved from a wide shear zone into a relatively narrow fault zone. During this phase, extensional and strike-slip deformation were completely decoupled from each other with NW–SE trending sinistral and NE–SW trending dextral strike-slip faults occurring alongside E-W trending normal faults. Extension was oriented NNW–SSE to NNE–SSW during this last phase.
The first rotational phase occurred since the Early-Middle Miocene and is characterized by an average net rotation of 23 ± 6° CW *(Uzel et al., 2015).* It is observed in Early Miocene deposits, often called the lower sequence (Fig 2). This was followed by an inversion of rotation during the second rotational phase which is characterized by an average net rotation of 22 ± 11° CCW *(Uzel et al., 2015).* These rotations are observed in Late Miocene rocks (Fig. 2), or upper sequence, which is separated from the lower sequence by a regional angular unconformity *(Sözbilir et al., 2011; Uzel et al., 2012, 2013).* This means the İBTZ region underwent a significant 45° CW rotation during the Early-Middle Miocene, followed by a 22° CCW rotation during the Late Miocene-Pliocene. In addition, a narrowing of the İBTZ was observed after the first rotational phase, similar to the transition from the second to third deformation phase.

## 2.4. The Soma basin

The Soma basin (Figs. 3 and 4) is one the NE-SW trending basins within the İBTZ. It was first thought to be an intramontane basin which developed in the topographic depressions related to Alpine deformation of the pre-Neogene basement rocks *(İncı, 1998, 2002).* However, most recent studies *(Uzel & Sozbilir, 2008; Uzel et al., 2012, 2013; Uzel, 2016)* found evidence for the occurrence of both major strike-slip and normal faulting in the İBTZ basins and therefore they interpret these basins as pull-apart basins. Overall, the stratigraphy of the Soma basin can be divided into three stratigraphic sequences separated by major unconformities. They are called from old to young the pre-Neogene rocks, Miocene volcano-sedimentary units and the Quaternary continental unit. The main focus of this research will be on the Miocene volcano-sedimentary units, because they were deposited and deformed during the main tectonic events that formed the İBTZ.

# 3. Method

Stratigraphic, structural and paleomagnetic analyses were used in this study to provide an integrated overview of the deformation history of the Soma basin. The study area is shown in figure 4. The resulting tectonic constraints from this area can then be compared with other parts of the İBTZ and western Anatolia.

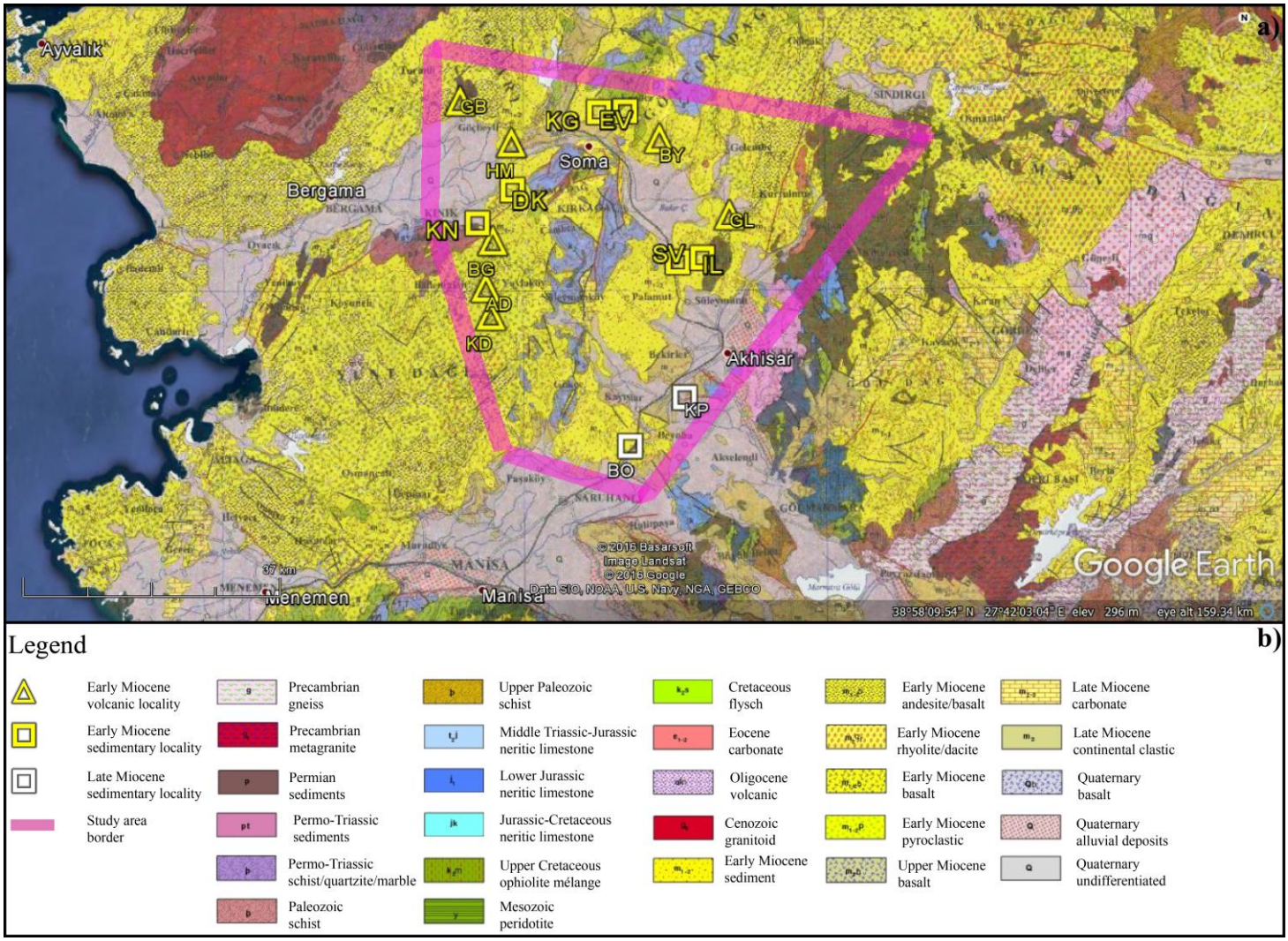


*Fig. 4: a) Geological map of Turkey with the study area of this research and paleomagnetic sampling locations indicated (after GDMRE, 2002; Google Earth v. 7.1.5.1557, 39° 7'45.43"N, 27°28'53.60"E, 2016). Abbreviations: AD = Arpadere, BG = Bağalan, BO = Beyoba, BY = Bayat, DK = Dereköy, EV = Evciler, GB = Göçbeyli, GL = Gelenbe, HM = Hamidiye, IL = Ilyaslar, KD = Karadere, KG = Küçükgüney, KN = Kınık, KP = Kapaklı, SV = Selvili; b) Legend*

## 3.1. Stratigraphy

Stratigraphic observations were mainly used to provide a framework for the structural and paleomagnetic results. In addition, the occurrence of volcanic activity within the stratigraphic sequence provides information about the timing of deformation phases.
Different stratigraphic sequences were subdivided using standard field-based analysis to constrain different lithologies as well as stratigraphic and structural contacts in the Soma basin. These observations will then be compared with the most recent age results and observations from previous studies. In this way, an up-to-date stratigraphic column can be constructed for the Soma basin.

## 3.2. Structural Geology

Field-based structural mapping and kinematic analysis was conducted to investigate the nature and order of deformation phases occurring in the Soma basin. The orientations of fault planes and fold axes, as well as cross-cutting relationships, provide constraints on different deformation phases when they are grouped in sets and mapped. On the other hand, kinematic indicators, such as slip directions and Riedel shear geometries, can be used to identify shear senses *(Fossen, 2010)*.
This information is used to compute the principal stress directions for each deformation phase. The computations were done using Win_TENSOR *(Delvaux & Sperner, 2003).* This software can be used to calculate the principal stress directions by deriving a contraction axis P, an extension axis T and a normal axis B from best-fit statistical analysis of the data *(Delvaux & Sperner, 2003; Sperner et al., 1993)*. To check the quality of the fault slip data, the ranking scheme from Delvaux & Sperner *(2003)* was used.
Finally, geological field cross-sections were used for determining relationships between different lithologies and structures.

## 3.3. Paleomagnetism

Paleomagnetic analysis of rocks is an effective method in determining the deformation history of strike-slip fault zones with prevailing simple shear conditions, like the İBTZ, because this analysis can constrain vertical-axis rotations with respect to the present-day geographic north *(Christie-Blick, 1985; Tauxe, 2010)*. In addition, analysis of the Anisotropy of Magnetic Susceptibility (AMS) in sediments provides constraints on principal stress directions for comparison with the structural data *(Hrouda, 1982; Tauxe, 2010).*
In total, we distinguished 44 Early Miocene volcanic sites distributed over 7 localities: Arpadere (AD), Bayat (BY), Bağalan (BG), Gelenbe (GL), Göçbeyli (GB), Hamidiye (HM) and Karadere (KD). Furthermore, we distinguished 20 Early Miocene sedimentary sites distributed over 6 localities: Dereköy (DK), Evciler (EV), Ilyaslar (IL), Kınık (KN), Küçükgüney (KG) and Selvili (SV). Finally, we distinguished 3 two Late Miocene sedimentary sites distributed over 2 localities: Beyoba (BO) and Kapaklı (KP). The distribution of all localities is shown in the geological map of figure 4. From these localities, 664 conventional paleomagnetic core plug samples were sampled using a gasoline-powered drilling machine, consisting of 338 volcanic samples and 326 sedimentary samples.
Volcanic rocks cool relatively fast and therefore retain spot readings of the geomagnetic field, while sedimentary rocks average out paleosecular variation due to relatively slow sedimentation rates, but their magnetic signal is overall weaker compared to volcanic rocks *(Tauxe, 2010).* Possible uncertainties in the sampling procedure are the fact that the sizes of tectonic blocks are not always well constrained, as well as the occurrence of several deformation phases in the study area. For these reasons, several sites from the same volcanic locality were sampled. In addition, all sampled localities are distributed as equally as possible over the study area and over different lithologies. Exception to this is the Soma open coal pit mine which contained no suitable outcrops, due to intense deformation. For measurement purposes, all samples were oriented using a magnetic compass and if possible, a sun compass for volcanic rocks. Furthermore, the bedding tilt was measured at every site to check whether a geographic or tectonic coordinate system yields more reliable directions. Core orientations and bedding tilts were corrected for the present-day declination of about 5° *(Thébault et al., 2015)*. In the laboratory, samples were cut to 22 millimeters for sedimentary cores and 11 millimeters for volcanic cores, due to their overall stronger magnetic signal.

### 3.3.1. Bulk Magnetic Susceptibility

The dominant magnetic carriers and chemical alterations of a selection of samples from different localities were determined by measuring their mass-normalized bulk magnetic susceptibility at increasing temperature steps. This was done using an AGICO KLY-3 (noise level $3.2*10^{-13}$ $Am^2$). The samples were powdered, weighted and put into a quartz-glass sample holder. The mass-normalized bulk magnetic susceptibility was measured during a number of heating and cooling cycles of 60°C starting at 180°C up to a maximum of 580°C.

### 3.3.2. Anisotropy of Magnetic Susceptibility

The Anisotropy of Magnetic Susceptibility (AMS) of a selection of sedimentary samples from all localities was measured to determine whether their magnetic fabrics have a mainly sedimentary or tectonic origin. In both cases, this will initially result in an oblate magnetic fabric with a minimum axis K3 perpendicular to the bedding. However, the maximum axis K1 of the AMS tensor will gradually be directed parallel to the orientation of maximum extension or equivalently perpendicular to the orientation of maximum compression upon deformation *(Hrouda, 1982).* This will result in separated K1 and K2 distributions in a tectonic fabric. The geological context is needed to determine whether the deformation was extensional or compressional in nature. In the case of a purely sedimentary fabric, the K1 and K2 axes will be indistinguishable. When the statistical measurement errors are too high, all three axes will be indistinguishable; these results were subsequently discarded.
The AMS tensor was measured and calculated using an AGICO Kappabridge MFK1-FA (noise level $2.1*10^{-13}$ $Am^2$). Jelinek statistics *(Jelinek, 1978, 1981)* were used for the calculations of the AMS tensor. The resulting data were viewed and interpreted using AGICO Anisoft 4.2.

### 3.3.3. Vertical-axis rotations

In order to determine the vertical-axis rotations, the samples were demagnetized stepwise in order to obtain the Characteristic Remanent Magnetization (ChRM) vectors. For most samples, this was done using thermal demagnetization. Volcanic samples were heated stepwise with increasing temperature increments of 20-50°C in an oven until they reached a temperature of 580°C, while most sedimentary samples were heated until they reached a temperature of about 420°C. At these maximum temperatures, the samples were sufficiently demagnetized to determine the ChRM, while thermal alteration due to overheating is avoided. In addition, some samples were demagnetized using alternating field (AF) demagnetization. These samples were placed manually in a Helmholtz coil to provide a non-magnetic environment. Stepwise increasing alternating fields of 10 mT were applied in three directions for all samples until a field of 60 mT was reached.
After each demagnetization step, the Natural Remanence Magnetization (NRM) of the sample was measured on a 2G Enterprise horizontal cryogenic magnetometer equipped with three DC SQUIDS (noise level $3.0*10^{-12}$ $Am^2$) or an AGICO JR6 spinner magnetometer (noise level $2.5*10^{-11}$ $Am^2$).
For all subsequent statistical paleomagnetic interpretations, the open-source and platform independent portal "Paleomagnetism.org" was used *(Koyman et al., 2016).* All measured samples were plotted in orthogonal demagnetization plots *(Zijderveld, 1967)* for interpretation. Characteristic components were derived from this using principal component analysis *(Kirschvink, 1980),* while standard Fisher statistics *(Fisher 1953)* were used to calculate mean directions and virtual geomagnetic pole (VGP) distributions with

corresponding dispersions (k, K) and cones of confidence (α95, A95). Thereafter, errors in declination ($\Delta D_{x)}$) and inclination ($\Delta I_x$) were calculated after Butler *(1992)*. A fixed 45° cut-off was applied to all sites which helped to determine which sites were used for constraining locality mean directions. Several samples with a (partial) overprint were interpreted using the great-circle approach from McFadden and McElhinny *(1988)*. Samples from tilted beds were corrected for their bedding plane. The A95 confidence envelope from Deenen et al. *(2011, 2014)* was used to determine whether a certain distribution represents paleosecular variation (PSV) or a spot-reading. In the latter case, $A95<A95_{min}$. When $A95>A95_{max}$, additional sources of scatter are present, such as small-scale rotational differences, chemical alteration or measurement errors. To determine whether two distributions with reversed polarities from the same locality share a Common True Mean Direction (CTMD), the Cartesian coordinate bootstrap test from Tauxe et al. *(2010)* was used. The fold test of Tauxe & Watson *(1994)* was used to check whether the magnetizations in a certain location were acquired before or after tilting. Both tests were applied whenever possible.

# 4. Results

## 4.1. Stratigraphy

Figure 5 shows an integrated stratigraphic column of the study area based on both available literature and own observations. The different sections will be described below.

### 4.1.1. Pre-Neogene basement rocks

The pre-Neogene rocks are considered as basement in the context of this study. This extremely deformed sequence consists of three units which are called the Bornova Flysch Zone, Sakarya Zone and the Başlamış Formation. All three basement units are found scattered across the Soma basin (Fig. 4). Example outcrops, as observed during this study, are shown in figure 6.
The Bornova Flysch Zone (Fig. 6a) is a highly deformed, NE-trending, olistostrome-mélange belt located between the MCC and the Karaburun Belt. It was formed during Cretaceous subduction in a foreland basin on the northern margin of the Anatolide-Tauride Block. This caused gravity-related mass flows, forming the olistostrome-mélange deposits *(Okay et al., 2012)*. Our observations indicate that these deposits are characterized by Mesozoic limestone and ophiolite blocks enclosed by sheared sandstones and shales of Cretaceous-Paleocene age in the Soma basin.
The Sakarya Zone (Fig. 6b) was observed in the Soma basin by this study as consisting of highly deformed, low-grade meta-sediments. These rocks are Permo-Triassic in age and are covered by an Upper Triassic-Jurassic sedimentary cover *(Bozkurt & Mittwede, 2001; Pickett & Robertson, 1996)*. The Sakarya Zone is part of the Rhodope-Vardar-Sakarya Zone orogenic belt which is found in parts of Turkey, Greece and Bulgaria. Most studies *(Jolivet et al., 2004; Okay et al., 2012; Ring et al., 1999)* interpret this orogenic belt as having been formed as part of an Alpine active margin during the Mesozoic. It subsequently underwent extension and exhumation.

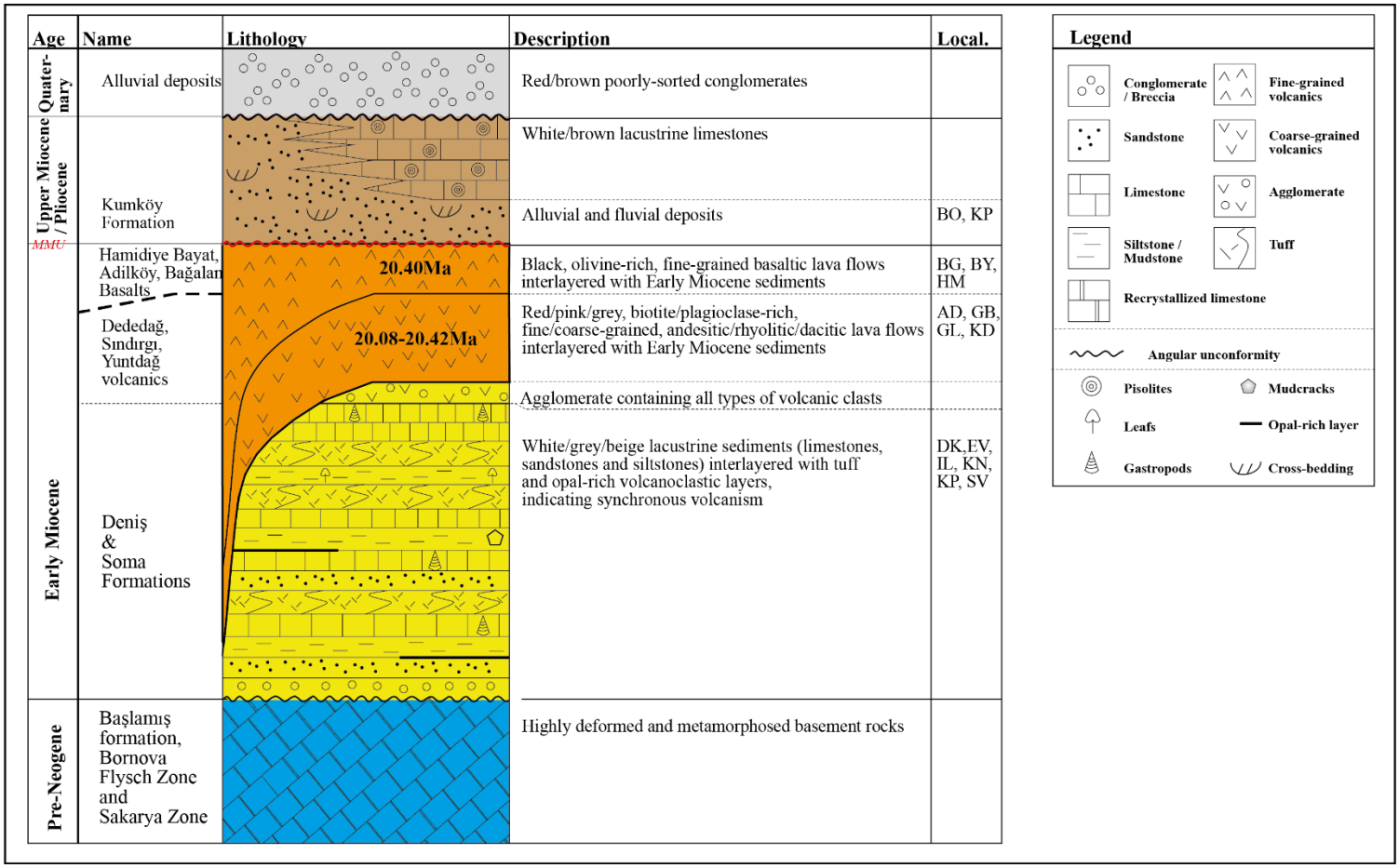


*Fig. 5: Integrated stratigraphic column of the Soma basin based on both own observations and previous research (Arpaliyiğit, 2004; Inci et al., 2002, 2003). The Middle Miocene Unconformity (MMU) is indicated in red. Volcanic ages are from Ersoy et al. (2014). The stratigraphic level of all sampled localities (Local.) by this study are indicated as well with the same abbreviations as in figure 4.*

On top of these Paleozoic and Mesozoic units, the sediments of the Eocene Başlamış Formation (Fig. 6c) were deposited. This formation is the oldest non-metamorphic rock unit as well as the youngest basement unit in the İBTZ *(Akdeniz & Tetkik, 1980)*. Our observations showed that the base of the Başlamış Formation is characterized by greenish conglomerates which were derived from ophiolites according to Akdeniz & Tetkik *(1980)*. After that, the sequence gradually fines upward into sandstones and finally marls alternated with greyish red-brown limestones. The limestones contain typical Eocene fossils, like nummulites, alveolinas, gastropods, bivalves and orbitolites. Therefore, we conclude that shallow marine conditions likely prevailed during the deposition of the Başlamış formation, with some influence of alluvial fans.


*Fig. 6: Basement lithologies in the Soma basin, as observed during this study: a) Bornova Flysch Zone; b) Sakarya Zone; c) Başlamış Formation.*

### 4.1.2. Miocene volcano-sedimentary units

The overlying Miocene volcano-sedimentary units are segregated from the basement rocks by a faulted contact or angular unconformity. Examples of these, as observed during this study, are displayed in figure 7.
The beginning of the sequence is characterized by alluvial fan conglomerates which were mainly deposited alongside the basin margins. Therefore, these deposits were likely derived from the topographic highs consisting of basement lithologies *(Inci, 2002)*. However, the sequence consists mainly of two volcano-sedimentary units which are separated by a regional angular unconformity, dividing them in a lower and upper sequence. This unconformity is Middle Miocene in age and is hence called the Middle Miocene unconformity or MMU *(Uzel et al., 2015; Uzel et al., 2016).* The sediments of the lower sequence are further subdivided into two formations which are called the Soma and Deniş formations *(Inci, 2002; Nebert, 1978).* Our observations indicate that both formations consist mainly of limestones alternating with sandstones, siltstones and marls, with the more resistant rocks often occurring as lenses (Fig. 8a). These deposits are interlayered with organic-rich, coal-bearing layers (Fig. 8b) as well as pyroclastic, biotite- and plagioclase-rich tuff and tuffite deposits (Fig. 8d). Grey or white mudstone is the most abundant type of limestone in both the lower and upper sequence in the Soma basin, but there are also gastropod-rich wackestone deposits (Fig. 8c). In organic-rich layers, fossil leafs can be found. Common sedimentary structures are mudcracks and loadcasts. These observations indicate that the dominant environment was fluvio-lacustrine throughout the deposition of the Soma and Deniş formations. Folding and faulting are also abundant in the lower sequence at different scales.

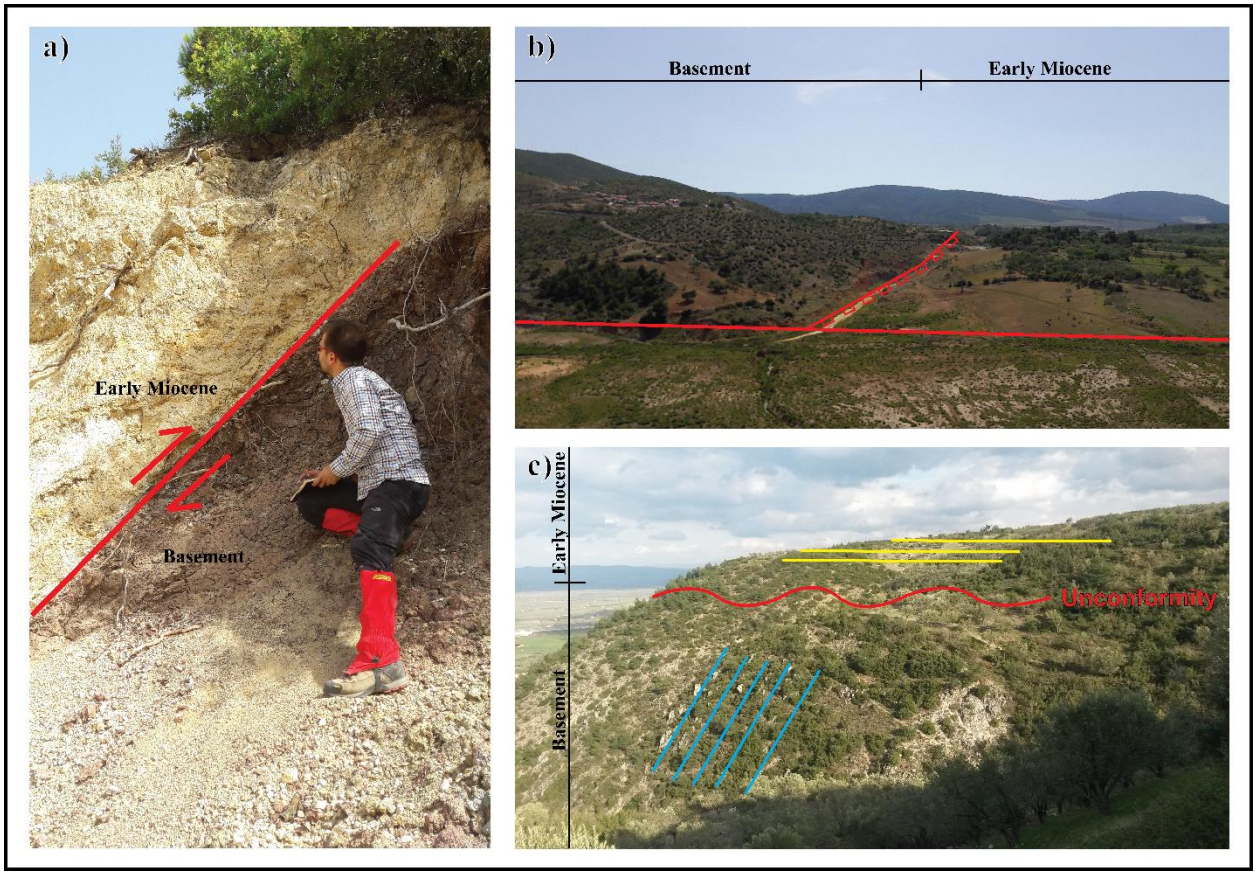


*Fig. 7: Contacts between the basement and Miocene deposits, as observed during this study: a) Faulted contact; b) Faulted contact alongside a topographic boundary; c) Angular unconformity with Bornova Flysch Zone basement deposits (blue) and Early Miocene deposits (yellow).*

Previously it was suggested that the MMU separated the Soma and Deniş formations *(Inci, 2002)*. However, Akgün et al. *(2007)* used dating of coals of the Miocene volcano-sedimentary unit to show that both the Soma and Deniş formation are Early Miocene in age. Dating of the volcanic extrusions within the study area by Ersoy et al. *(2014)* appears to confirm this. The age results from volcanic extrusions occurring in the study area are shown in Table 1 (Appendix 1). Our observations indicate a subdivision of the extrusions into two distinct categories: pinkish to greyish, coarse grained, biotite- and plagioclase-rich andesites and rhyolites (Fig. 9a) and black to greyish, fine grained, olivine-rich, basalts and trachybasalts which regularly occur as columnar joints (Fig. 9b). Both types can contain gas bubbles. The occurrence of andesites is an indication that volcanic activity was linked to subduction. On the other hand, the similar age of both distinct types of observed extrusions suggests that volcanism was bimodal in nature. This indicates that volcanic activity can also be related to partial melting of continental crust during a transtensional deformation phase *(Till et al., 2007)*. According to our field observations, the extrusions are interlayering with the sediments of the Soma and Deniş formations, confirming the results from Akgün et al. *(2007)* and Ersoy et al. *(2014)*. Extrusions proximal to the Yuntdağ and Sındırgı volcanic complexes are mostly large-scale, covering the entire lower sequence succession. The separate extrusions are often underlain by agglomerate deposits (Fig. 9d) containing clasts of both types of volcanic rocks. In other cases, there is a direct contact between extrusion and sediment, which can result in baked contacts (Fig. 9c).
Using this information, it appears that the MMU separates the overlying Late Miocene-Pliocene Kumköy formation from the Soma and Deniş formations. The Kumköy formation is

hence considered as the sedimentary succession of the upper sequence in the Soma basin. Our observations show that this formation consists of alluvial and braided river conglomerate, sandstone and siltstone deposits with soft-sediment loadcasting (Fig. 10a) and cross-bedding (Fig. 10b), as well as pisolite-rich lacustrine carbonates. This indicates that the environment during the deposition of the Kumköy formation was still fluvio-lacustrine, but with more evaporitic conditions. Faulting and folding are less pronounced in the upper sequence compared to the lower sequence.


*Fig. 8: Several lower sequence deposits and sedimentary structures within the Soma basin, as observed during this study: a) Typical lower sequence deposits at Selvili (SV); b) Coal-bearing deposits; c) gastropods at Evciler (EV); d) Ash-bearing deposits at Selvili (SV).*

### 4.1.3. Quaternary continental unit

The most recent deposits are sediments of the Quaternary continental unit *(İnci, 2002)*. Our observations show that they mainly consist of reddish-brown apron and alluvial fan deposits which rest unconformably with an erosional surface on top of the older units. In addition, they contain clasts derived from lower sequence lithologies.


*Fig. 9: Types of volcanism within the Soma basin, as observed during this study: a) Coarse-grained rhyolitic extrusion at Gelenbe (GL); b) Fine-grained basaltic extrusion at Bağalan (BG); c) Baked contact with sediments at Hamidiye (HM); d) Agglomerate deposit.*


*Fig. 10: Several upper sequence deposits and sedimentary structures within the Soma basin, as observed during this study: a) Lacustrine limestone with loadcasting at Kapaklı (KP); b) Fluvial siltstone containing cross-bedding and conglomerate lenses.*

## 4.2. Structural Geology

Additions and adjustments were made to the geological map from GDMRE *(2002)* based on the structural mapping of this study and the geological map from Inci et al. *(2003)*. The resulting geological map of the study area is shown in figure 11. In the sections below, the newly acquired structural and kinematic data from the Soma basin will be presented.

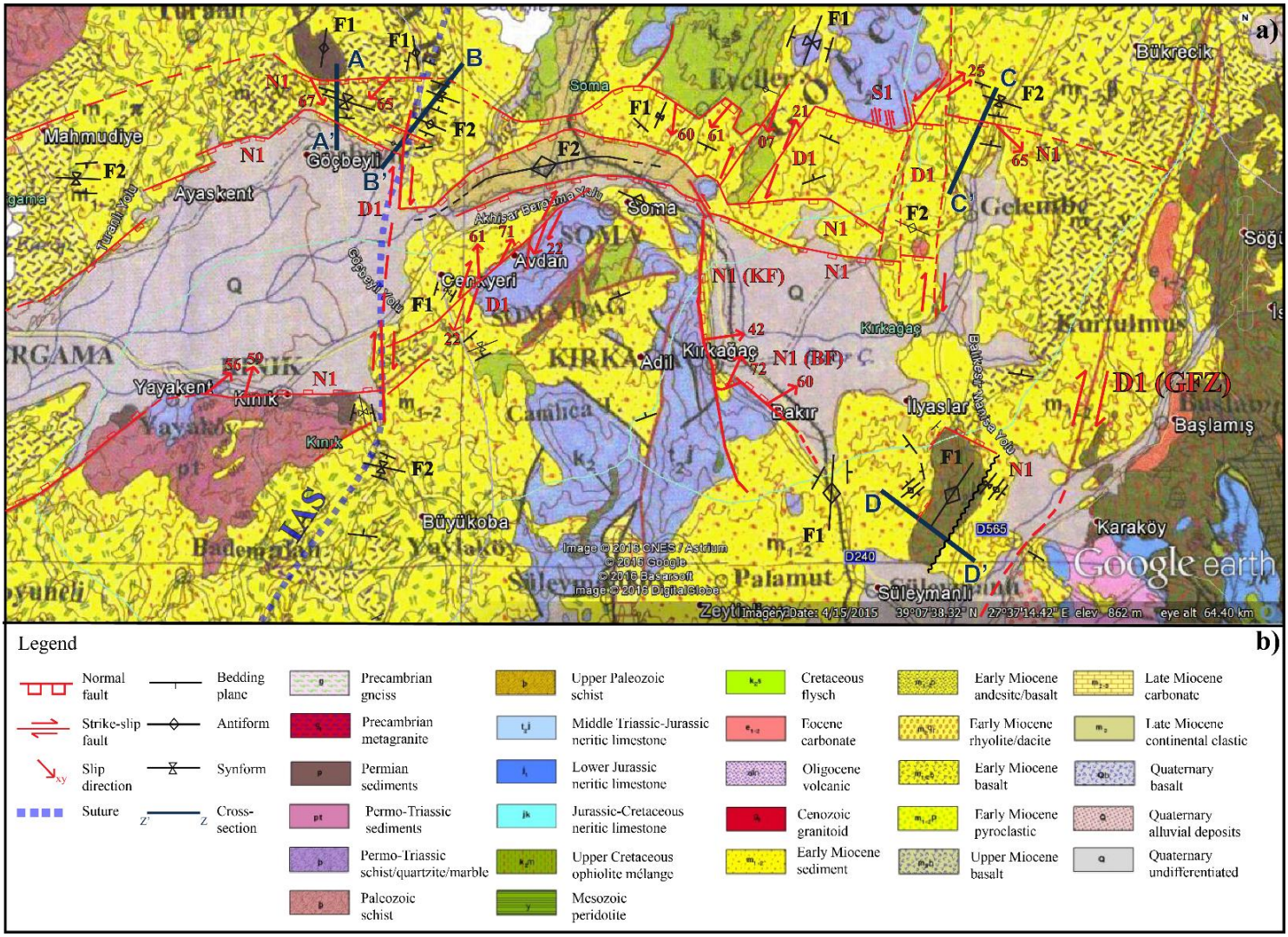


*Fig. 11: a) Structural geological map of the Soma basin based on observations from this study. Fault and fold sets (Figs. 12-15) are indicated as well (after GDMRE, 2002; Google Earth v. 7.1.5.1557, 39° 7'45.43"N, 27°28'53.60"E, 2016). Abbreviations: GFZ = Gelenbe Fault Zone, IAS = İzmir-Ankara Suture, BF = Bakır Fault, KF = Kirkağaç Fault; b) Legend.*

### 4.2.1. Faults

Careful grouping of the observed faults within the Soma basin resulted in three general fault sets within the Soma basin: NE-SW trending dextral strike-slip, NW-SE trending sinistral strike-slip faults and E-W trending normal faults, faults. These three fault sets are henceforth called D1, S1 and N1. All fault data is listed in respectively Table 2, 3 and 4. In the same order, figures 12, 13 and 14 display the fault-slip data for each set, alongside the computed Rose diagrams, principal stress directions and the quality test from Delvaux & Sperner *(2003)*. Principal stress analysis could not be done for S1, because too few results were obtained for this set (Fig. 13c).
D1 faults are characterized by NE-SW trending fault planes, high dip angles and small oblique normal components. The principal stresses from this fault set indicate that they were formed under NNW-SSE trending extension and WSW-ESE trending compression (Fig. 12c). Some D1 faults are superimposed on older structural features, for example the Neo-Tethyan İzmir-Ankara Suture (IAS) from Okay & Siyako *(1993)*, as visible in figure 11. D1 faults

generally cross-cut the basement and lower sequence deposits. The same is true for S1 faults. However, these faults generally have a larger normal component compared to D1 (Fig. 13a). S1 slip directions generally follow a NW-SE trend (Fig. 13).

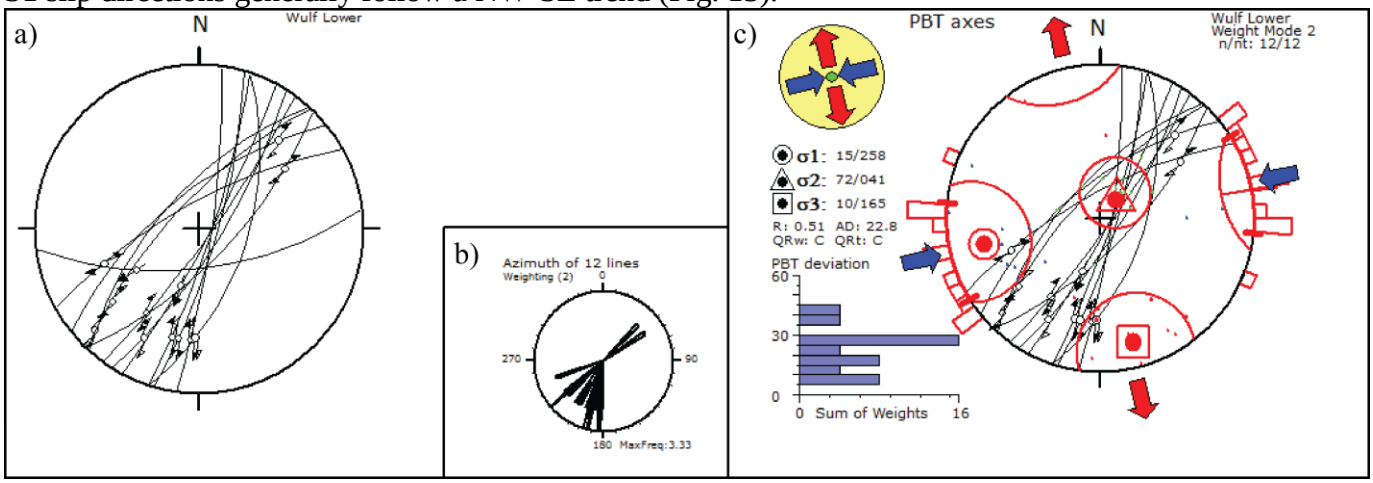


*Fig. 12: a) D1 fault planes and slip directions projected on a lower-hemisphere Wulff net; b) Rose diagram of fault set D1; c) PBT axes (with circle/triangle/square representing $\sigma_1/\sigma_2/\sigma_3$) and principal stress directions (red/blue arrows) for D1, determined using Win_TENSOR (Delvaux & Sperner, 2003). Abbreviations: QRw/QRt = quality rank from Delvaux and Sperner (2003) on a scale from A (best) to E (worst), n = number used fault-slip data in determining the principal stress directions after best-fit statistical analysis, nt = the total number of fault-slip data, AD = angular deviation, R = ratio of principal stress differences $(\sigma_2-\sigma_3)/(\sigma_1-\sigma_3)$.*

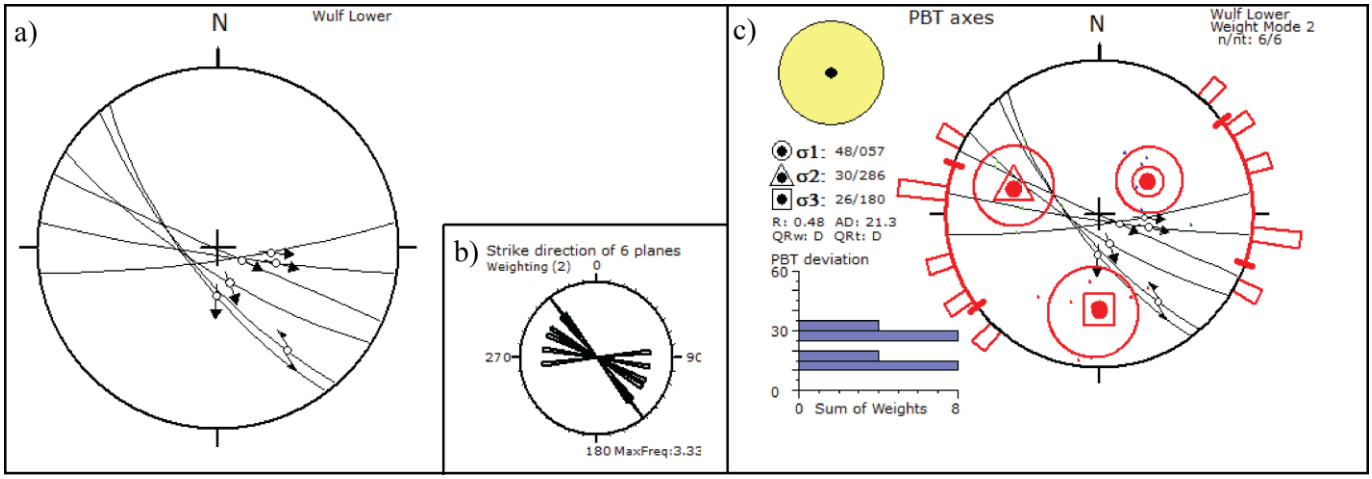


*Fig. 13: a) S1 fault planes and slip directions projected on a lower-hemisphere Wulff net; b) Rose diagram of fault set D1; c) PBT axes (with circle/triangle/square representing $\sigma_1/\sigma_2/\sigma_3$) and principal stress directions (red/blue arrows) for S1, determined using Win_TENSOR (Delvaux & Sperner, 2003). Abbreviations: QRw/QRt = quality rank from Delvaux and Sperner (2003) on a scale from A (best) to E (worst), n = number used fault-slip data in determining the principal stress directions after best-fit statistical analysis, nt = the total number of fault-slip data, AD = angular deviation, R = ratio of principal stress differences $(\sigma_2-\sigma_3)/(\sigma_1-\sigma_3)$.*

N1 faults have a generally high dip angle, often larger than 60°. This could be an indication for a listric fault geometry or reactivation. Most have an oblique component and are E-W oriented with approximately N-S trending extension (Fig. 14c). The most notable exceptions on this are the large-scale Bakır and Kirkağaç faults which have NW-SE trending fault planes

(Table 4). N1 faults are observed cross-cutting the whole sedimentary succession. In addition, they cut and displace D1 and S1 faults (Fig. 11). Only the large-scale D1 Gelenbe Fault Zone (GFZ) remains relatively undisturbed in this aspect. Remarkably, the GFZ is still active at present *(İnan et al., 2012).*

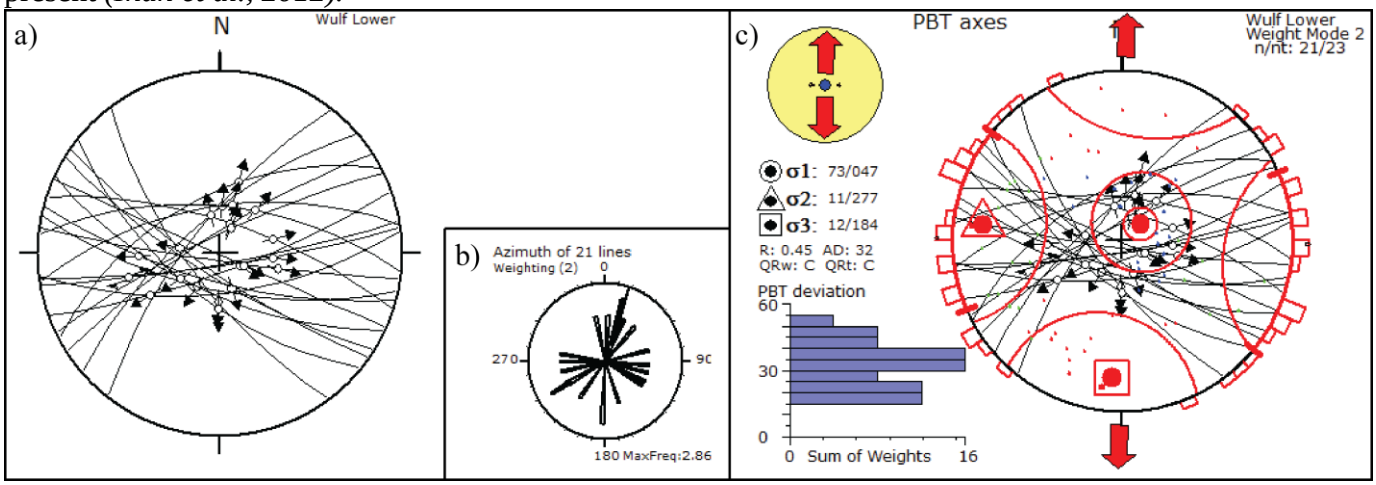


*Fig. 14: a) N1 fault planes and slip directions projected on a lower-hemisphere Wulff net; b) Rose diagram of fault set D1; c) PBT axes (with circle/triangle/square representing $\sigma_1/\sigma_2/\sigma_3$) and principal stress directions (red/blue arrows) for N1, determined using Win_TENSOR (Delvaux & Sperner, 2003). Abbreviations: QRw/QRt = quality rank from Delvaux and Sperner (2003) on a scale from A (best) to E (worst), n = number used fault-slip data in determining the principal stress directions after best-fit statistical analysis, nt = the total number of fault-slip data, AD = angular deviation, R = ratio of principal stress differences $(\sigma_2-\sigma_3)/(\sigma_1-\sigma_3)$.*

### 4.2.2. Folds

Two distinct fold axis orientations can be observed on the geological map of figure 11. The first set of folds has an approximately NNW-SSE trend, indicating ENE-WSW trending compression. This fold set is henceforth called F1. Folds from this set can be observed in basement to lower sequence deposits. Furthermore, F1 folds are often cut and displaced by N1 faults. Figure 15 shows some observed N-S trending folds in lower sequence sediments. The second fold set is hence called F2. This set has an approximately WNW-ESE trend, indicating NNE-SSW trending compression. Folds from this set deform deposits from both the lower and upper sequence.


*Fig. 15: Two N-S trending folds from fold set F1, as observed in the study area, close to: a) Küçükgüney (KG); b) Dereköy (DK).*

### 4.2.3. Geological field cross-sections

Four schematic geological field cross-sections were made in the Soma basins. They are shown in figure 16; the locations of these cross-sections are indicated in figure 11. Several important observations can be made from these cross-sections. The largest-scale listric N1 faults often result in topographic boundaries between the different sedimentary units of the Soma basin with the basement units often on topographic highs. This is an indication for a basin-and-range type of structural style within the Soma basin, where the listric N1 faults act as detachments. In addition to this, there are differences in the amount of faults and deposits which they cross-cut between cross-sections A-A' and B-B', despite their proximity to each other. This could be an indication for a difference in accommodation space related to earlier deformation phases. Furthermore, it can be inferred from cross-sections B-B' and D-D' that N1 faults cut and displace F1 folds, because layers folded by F1 are offset by N1 faults. Finally, it is visible that the Early Miocene volcanics are folded and interlayering with the sediments from the Soma and Deniş formations. This is in accordance with the results from Ersoy et al. *(2014)*.

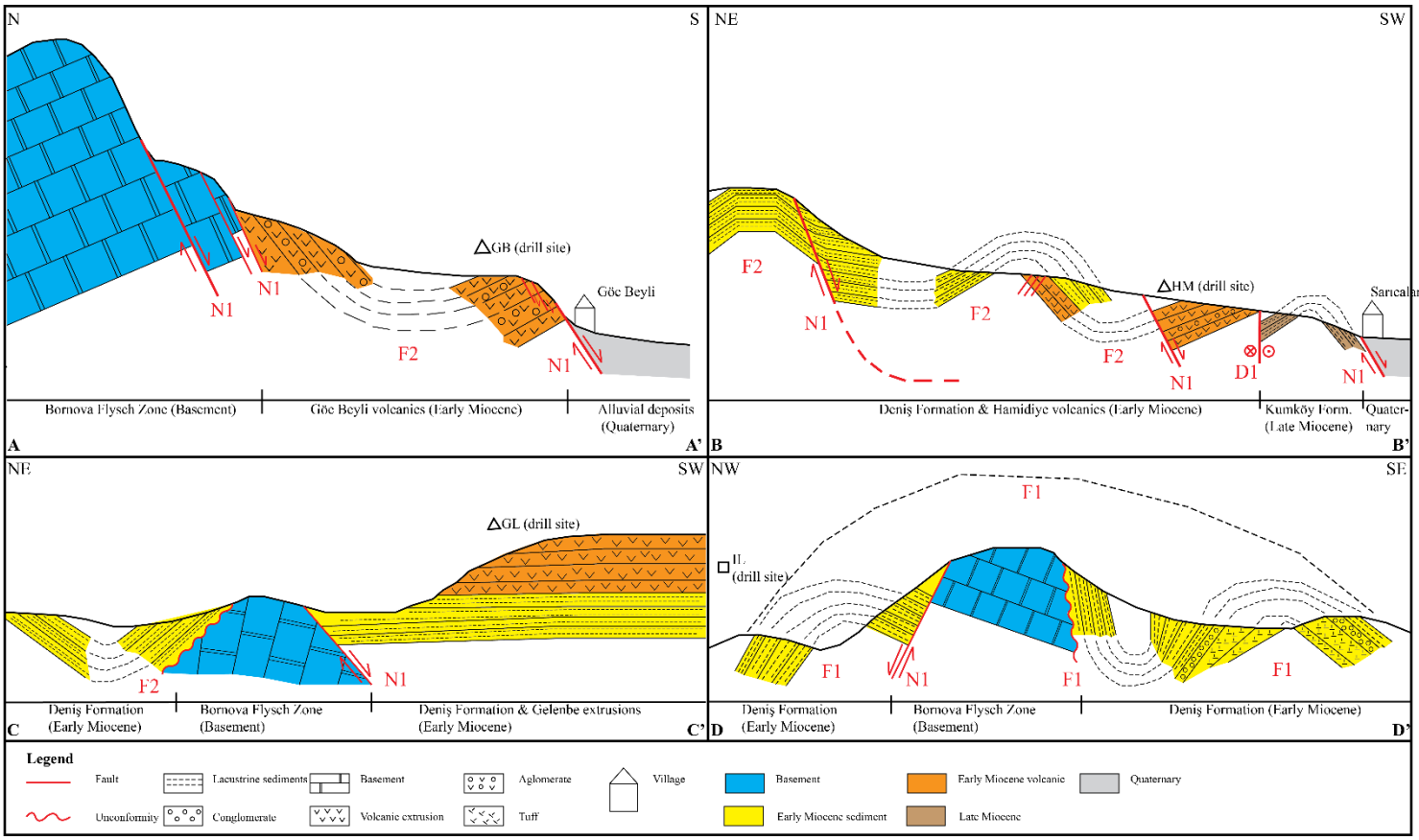


*Fig. 16: Schematic geological field cross-sections A-A', B-B', C-C', D-D'. Corresponding fault and fold sets are indicated, as well as sampled localities. Locations are drawn on Fig. 11. Drill site abbreviations are listed in figure 4.*

## 4.3. Paleomagnetism

### 4.3.1. Bulk magnetic susceptibility

The mass-normalized bulk magnetic susceptibility for four representative volcanic samples and two sedimentary samples from different localities are shown in figure 17 at seven consecutive heating and cooling cycles. Plots of intensity decay during thermal demagnetization are indicated as well for comparison.
Andesitic sample AD06.3 shows a gradually increasing susceptibility up to 360°C with only minor susceptibility changes during the first five heating cycles. These minor changes are likely related to chemical alteration due to low temperature oxidation. Between 360°C and 420°C, the susceptibility reaches a maximum. This maximum can be interpreted as a Hopkinson peak which marks the transition from blocking temperatures to Curie temperatures for magnetic minerals in the sample *(Hopkinson, 1989)*. The sharp susceptibility drop associated with the Curie temperature is observed afterwards. The susceptibility reaches a minimum at 580°C which seems to indicate that magnetite ($Fe_3O_4$) is the dominant magnetic carrier. However, the inflexion of the curve towards a slower decrease in susceptibility around 550°C indicates that rather Ti-poor titanomagnetite ($Fe_2TiO_4$) is the dominant magnetic carrier, as the relative amount of titanium in magnetite leads to a gradual decrease in Curie temperature *(Dunlop and Özdemir, 1997)*. The final cooling step is characterized by lower susceptibilities compared to the first heating cycles, indicating that the sample underwent further oxidation. These observations correspond well to the intensity decay curve of AD06.3. This curve also shows a gradual decrease at first, followed by faster decrease after 400°C and a minimum intensity at 580°C.
KD02.2 is another andesitic sample. The overall properties of this sample are generally the same as AD06.3, also displaying a sharp drop in susceptibility above 420°C. However, the inflexion related to the presence of Ti-poor titanomagnetite occurs at a lower temperature of around 530°C in this sample, indicating a slightly larger amount of titanium. Furthermore, the Hopkinson peak is less clear, occurring at around 310°C. Afterwards, the susceptibility starts to gradually decrease. These observations could indicate the presence of maghemite or a higher degree of chemical alteration compared to AD06.3. The susceptibility curve of KD02.2 again correspond nicely to its intensity decay curve.
GL02.1 is a rhyolitic sample, where (titano)magnetite is again the dominant magnetic carrier. However, the minimum susceptibility around 580°C is substantially higher compared to AD06.3 and KD02.2. Furthermore, large susceptibility drops can be observed after each heating cycle beyond 360°C. Both of these properties are an indication for the inversion of maghemite ($\gamma Fe_2O_3$) to hematite ($Fe_2O_3$), starting at 360°C *(Dankers, 1978)*. The presence of maghemite could be an indication for a high degree of weathering, related to low temperature oxidation *(Dunlop and Özdemir, 1997)*. This could have resulted in partial overprint of the magnetization.
BY01.7 is the final volcanic sample and basaltic in composition. It has a clearly defined Hopkinson peak at 360°C. Its behaviour after this peak is characteristic for the presence of Ti-poor titanomagnetite as dominant magnetic carrier. This can also be very clearly observed in the intensity decay curve, where a very sharp drop in intensity occurs at 400°C. Furthermore, the susceptibility values of BY01.7 are almost completely reversible after each cooling step, indicating a low amount of chemical alteration.
SV01.1 is a sedimentary specimen, composed of tuffite. It is characterized by relatively low intensity values, resulting in a noisy susceptibility curve. A maximum value is reached at 240°C, which can be interpreted as a Hopkinson peak. Afterwards, susceptibility gradually decreases during each subsequent heating step. An inflexion of the curve towards faster

susceptibility decrease can be observed at 360 °C, indicating the occurrence of maghemite and its associated inversion.

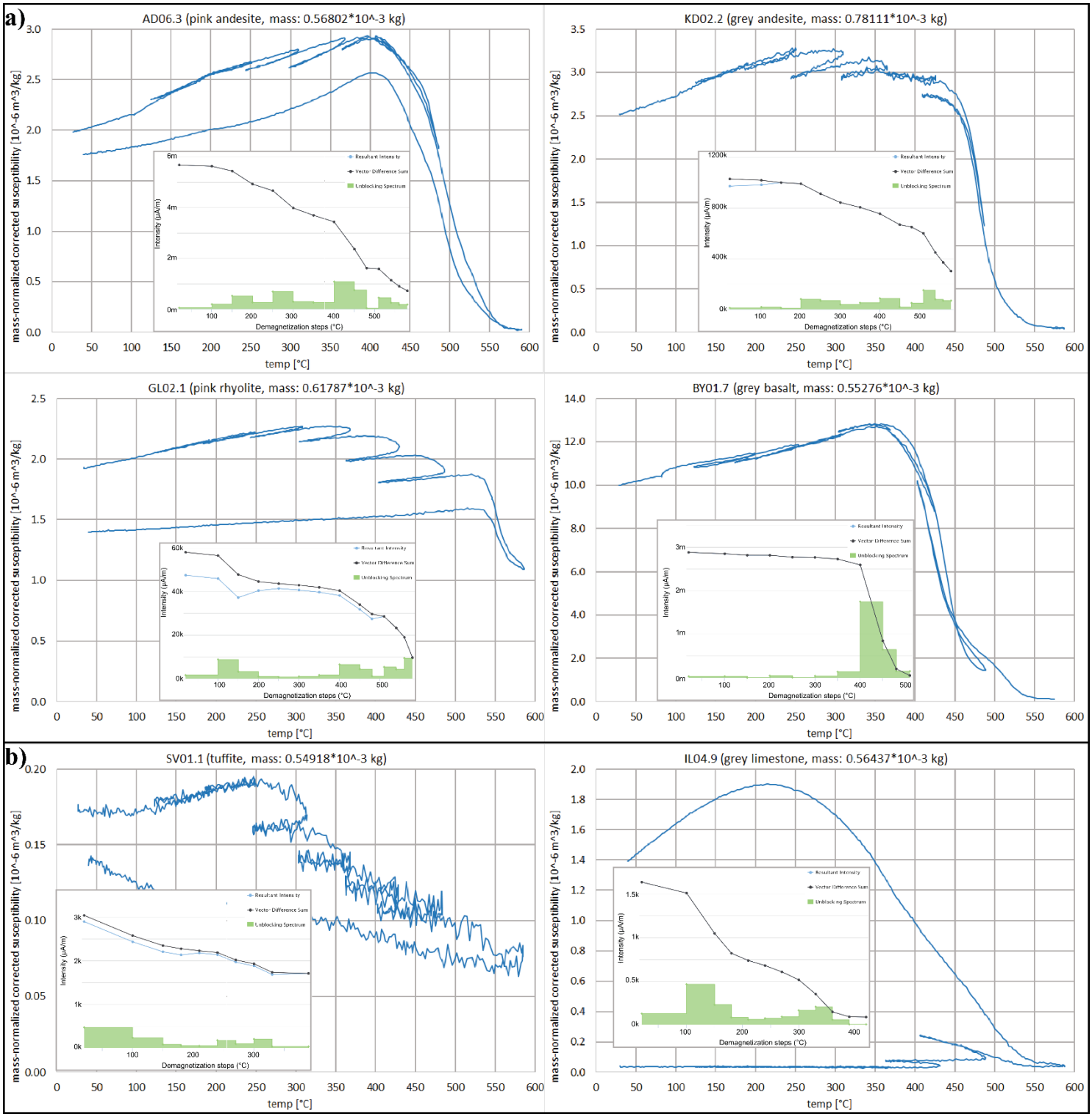


*Fig. 17: Representative temperature versus bulk magnetic susceptibility curves during seven heating and cooling steps of 60°C starting at 180°C up to a maximum of 580°C for 4 volcanic (a) and 2 sedimentary (b) samples. Temperature is listed in °C and bulk magnetic susceptibility in $10^{-6}$ $m^3/kg$. Corresponding intensity decay plots are shown as well with: black line = vector difference sum, blue line = resultant intensity, green = unblocking spectrum.*

The final sample IL04.9 is a greyish-white limestone from the lower sequence. It has a generally low magnetic susceptibility until a temperature of 390°C is reached. At this point, the susceptibility increases after each heating step. Such behaviour is common for a sample containing pyrite ($FeS_2$). Pyrite is a paramagnetic mineral, but it oxidizes to ferromagnetic magnetite around 390°C, resulting in an increase in susceptibility *(Van Velzen & Zijderveld, 1992)*. Pyrite is a common mineral in organic-rich, oxygen-poor environments with a supply of iron. Therefore, its presence in IL04.9 is another indication that lower sequence limestones were formed in a fluvio-lacustrine environment. The formation of magnetite does not disturb the determination of the ChRM of IL04.9, because thermal demagnetization up until 420°C was sufficient to obtain a reliable direction, as evidenced by the intensity decay curve.

### 4.3.2. Anisotropy of Magnetic Susceptibility

The Anisotropy of Magnetic Susceptibility (AMS) of a selection of samples from all sedimentary localities was measured. The measurement errors in samples from most localities were too high, resulting in undistinguishable fabrics for those localities. The large errors may be attributed to low overall intensities of the samples. Therefore, these localities were discarded. Only three localities (Evciler, Kapaklı and Selvili) yielded results with low measurement errors, resulting in a largely sedimentary fabric after bedding correction. The resulting AMS ellipsoids of these three localities are shown in figure 18, alongside their inferred principal stress directions. In all three cases, K3 is oriented vertically to the bedding plane within its error margin. Furthermore, the K1 and K2 axes form a girdle perpendicular to the K3-axis, resulting in an oblate AMS ellipsoid.
Evciler (Fig. 18a) and Selvili (Fig. 18b) show a primarily tectonic fabric, where K1 and K2 measurements form well-defined clusters. All three axes have the same general orientation in both localities, indicating approximately N-S trending extension parallel to K1 or equivalent E-W trending compression parallel to K2. The same orientations can be inferred from Kapaklı (Fig. 18c). However, the K1 and K2 directions of this locality exhibits a considerable overlap, resulting in a non-significant difference between them. This could be an indication for a non-tectonic fabric. However, it could also be generated by measurement errors. In any case, they do not contradict the results from Evciler and Selvili. Therefore, the AMS results indicate a consistent N-S trending extension or equivalent E-W trending compression in the Soma basin. When comparing both options with the fault slip data (Figs. 12 and 14), as well as the geological map and field cross-sections (Figs. 11 and 16), we conclude that N-S trending extension is the most plausible option.

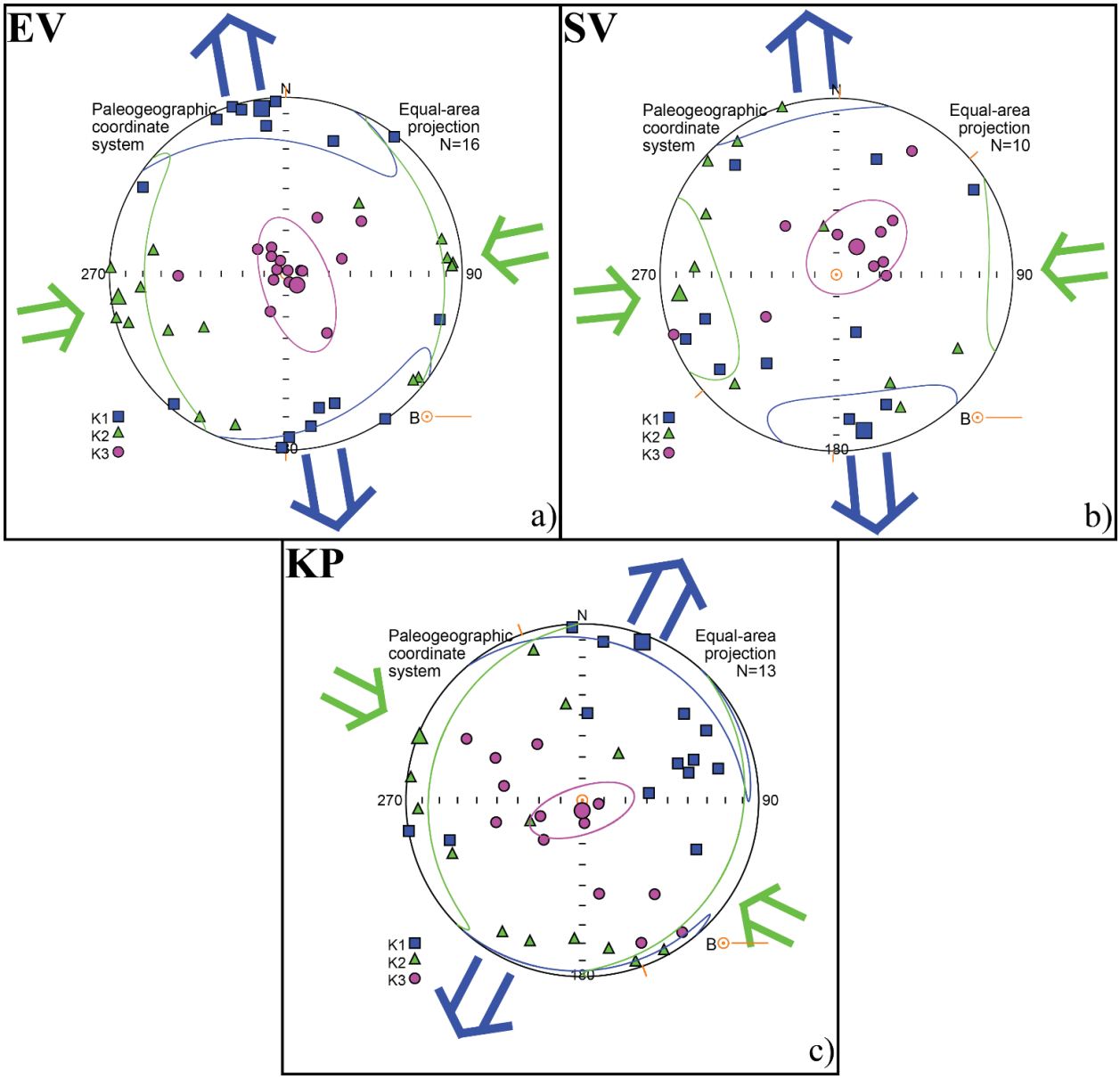


*Fig. 18: Anisotropy of Magnetic Susceptibility results for three localities in the Soma basin in a paleogeographic coordinate system and equal area projection: a) Evciler; b) Selvili; c) Kapaklı. N equals the number of used samples for each locality. K1/K2/K3 results are indicated with a blue square/green triangle/pink circle. Mean axes and corresponding confidence envelopes are shown as well. Bedding planes are indicated with orange lines. Resulting principal stress directions $\sigma_1/\sigma_2$ are indicated with blue/green arrows.*

### 4.3.3. Vertical-axis rotations

In total, 432 samples were demagnetized to obtain their ChRM directions. In many samples a small viscous component is removed during the first few demagnetization steps. The mean paleomagnetic data for every measured site is listed per locality in Table 5 in both a geographic and tectonic reference frame. The average declination D and its error $\Delta D_x$ from each locality were used in describing the vertical-axis rotations. Figure 19 shows representative orthogonal demagnetization plots *(Zijderveld, 1967)* for both volcanic and sedimentary samples. Example plots from Beyoba (BO) and Kapaklı (KP) are indicated as well (Fig. 19c). The results from these Late Miocene localities were not reliable due to the

low intensities of the samples (Fig. 19d); they were subsequently discarded. Figure 20 shows the equal area projections of the ChRM directions for all remaining Early Miocene localities. Arpadere (AD), Bağalan (BG), Dereköy (DK), Karadere (KD) and Kınık (KN) are all sampled localities from the south-western quadrant of the study area (Fig. 4). Karadere is the south-westernmost location, consisting of nine volcanic (andesitic) sites as part of the Yuntdağ volcanic complex (Table 1). It yields a coherent clockwise (CW) rotation of 30 ± 9°. Arpadere is located just north of Karadere, also being part of the Yuntdağ volcanic complex. Seven extrusions were sampled at this locality. It exhibits a well-determined CW rotation of 24 ± 10°. The only exception on this is site AD02 which was consequently discarded after applying a 45° cut-off. The A95 values of both Arpadere and Karadere fall into the A95 confidence envelope of Deenen et al. *(2011, 2014)*, therefore not underrepresenting PSV. The low uncertainties can be attributed to the strong magnetic signal of titanomagnetite as well as the low degree of weathering, as evidenced by the bulk magnetic susceptibility results (Fig. 17). Application of the fold test yielded a negative result for both Karadere and Arpadere, indicating that the characteristic components of these localities were acquired after folding. Therefore, a geographic reference frame yields the best fit for both localities. The fold test of Arpadere is shown in figure 21a. Bağalan is another volcanic locality in the south-western quadrant of the study area, consisting of three columnar basaltic sites. This locality yields a non-significant rotation of 5 ± 30° CCW when BG02 is discarded after a 45° cut-off. The large $\Delta D_x$, as well as the steep inclination (75°) can be attributed to the low amount of two sampled sites. A tectonic correction was applied to Bağalan, because this resulted in a better fit with the consistent results from Arpadere and Karadere. Dereköy and Kınık are two sedimentary localities in the south-western quadrant of the study area. KN01 is the only used site from Kınık. The other three sites from this locality have quite scattered directions ($k<10$) and are therefore not used for the final result. The average $\Delta D_x$ and A95 values from Kınık become slightly lower after tectonic correction. In addition, this resulted in a better fit with the results from the previous three localities, producing a CW rotation of 51 ± 20°. The same is true for Dereköy, who produces a CW rotation of 42 ± 9° after tectonic correction. In addition, Dereköy yields a shallow inclination of 28° in a geographic reference frame. If we combine the results of all five south-western localities, a coherent CW net rotation of 34 ± 7° is produced (Fig. 20a). Therefore, these localities are most likely part of a rigid block which is henceforth called the Kınık tectonic block.

Selvili (SV), Ilyaslar (IL) and Gelenbe (GL) are all three sampled localities in the eastern part of the study area, separated from the south-western localities by abundant faulting (Figs. 4 and 11). Selvili consists of two sites, composed of lower sequence fluvio-lacustrine and pyroclastic deposits, which form an anticline. Unfortunately, the results are too scattered to produce a reliable fold test for this locality. However, the data seems the most plausible before tectonic correction, producing a CW rotation of 28 ± 14°, because tectonic correction results in a shallow inclination (25°) and a low k value (7.6) which indicates a high amount of scatter. Ilyaslar is part of the same sedimentary sequence as Selvili. It also underwent a CW rotation of 25 ± 6° after discarding IL02 due to its unrealistic direction, combining a southward pointing declination with a shallow, downward pointing inclination. The fold test for Ilyaslar is negative (Fig. 21b), indicating post-tilt magnetization. Therefore, a geographic reference frame was chosen for this locality. Gelenbe consists of six horizontally deposited rhyolitic extrusions, originating from the Sındırgı volcanic complex (Table 1). Gelenbe is characterized by large scatter, yielding a rotation of 19 ± 32°. Furthermore, its A95 value is higher than $A95_{max}$, indicating an additional source of error. This could be related to overprint due to chemical alteration, as evidenced by the presence of maghemite in representative samples from Gelenbe, indicating a high degree of weathering (Fig. 17). If we combine all three eastern localities, a coherent 27 ± 6° CW rotation is produced (Fig. 20b). Therefore,

these localities likely represent another rigid block which is henceforth called the Bakır tectonic block (Fig. 20b). The Kınık and Bakır tectonic blocks have the same rotation within their error margins. All data of both tectonic blocks is listed in Table 6.
The remaining five locations in the northern part of the study area do not yield a consistent rotational pattern (Fig. 20c). Furthermore, these locations often have large $\Delta D_x$ values. The only exception on this is Evciler (EV), which mainly consists of grey organic mudstones. It exhibits low amounts of scatter in both a geographic and tectonic reference frame. However, the inclination is shallow (28°) before tectonic correction. Therefore, a tectonic reference frame was chosen for Evciler, producing a CW rotation of 60 ± 8°. In addition, EV01 and EV04 have reversed polarities, while EV02 and EV03 have normal polarities. This provided an opportunity for a reversal test. Figure 22 shows the resulting test using the coordinate bootstrap of Tauxe et al. *(2010)*. The overlapping confidence intervals for all three axes indicate that the normal and reversed sites from Evciler share a CTMD.
Bayat (BY) and Göçbeyli (GB) are two predominantly volcanic locations in the northern part of the Soma basin (Fig 4.), consisting of respectively six and nine sites. Both of them underwent non-significant CW rotations of respectively 4 ± 28° and 16 ± 15°, since the $\Delta D_x$ values are high, although it becomes less after tectonic correction for Bayat. On the other hand, Göçbeyli (GB) produces a very shallow inclination (-7°) after tectonic correction. Therefore, a geographic reference frame results in a better fit for Göçbeyli. BY06 is the only sedimentary site from Bayat, while the others consist of columnar basalts. BY06 did not produce reliable results (k=5.7) and was subsequently discarded. The same is true for volcanic sites GB05 and GB06 from Göçbeyli who both produced chaotic directions with k values of respectively 4.2 and 5.8. In the case of the latter two, the chaotic directions could be related to lightning strikes. Lightning strikes are typically characterized by chaotic directions, strong magnetizations, straight lines to the origin or initially fast decay of the NRM. These features are clearly visible in the orthogonal demagnetization (Fig. 19c) and intensity plots (Fig 19d) of an example specimen from GB06.
Küçükgüney (KG) is the last sedimentary locality within the Soma basin, situated close to Evciler (Fig. 4). It produced only five reliable samples from one site, resulting in a CCW rotation of 27 ± 21°. A tectonic reference frame was used for Küçükgüney, because this resulted in a more realistic inclination of 65°. The contrasting CCW rotation compared to the CW rotation from the neighbouring Evciler, alongside the low amount of reliable samples and the large $\Delta D_x$ value, indicate that the results from Küçükgüney are not representative for the Soma basin.
Hamidiye (HM) is the final sampled locality in this study, consisting of five volcanic extrusions and one sedimentary tuff site. HM06 produced unrealistic directions, combining a southward pointing declination with a downward pointing inclination. It was subsequently discarded after application of a 45° cut-off. A geographic reference frame was used for Hamidiye, because the k and A95 values became slightly higher and the inclination slightly lower after tectonic correction. This resulted in a strikingly different CCW rotation of 22 ± 14° compared to the CW rotation of the neighbouring Göçbeyli (Fig. 4).
All resulting rotations from this study are shown per locality in figure 23a. Furthermore, the two resulting tectonic blocks are shown in figure 23b, alongside revisited data from Uzel et al. *(2015)* and van Hinsbergen et al. *(2010)*. Uzel et al. *(2015)* constrained average net rotations of 23 ± 6° CW and 23 ± 10° CCW for the whole İBTZ and Menderes region respectively. These results are indicated in figure 23b as well. The average net rotation of the Soma basin during the Early Miocene equals 29 ± 8° CW when all localities are averaged.

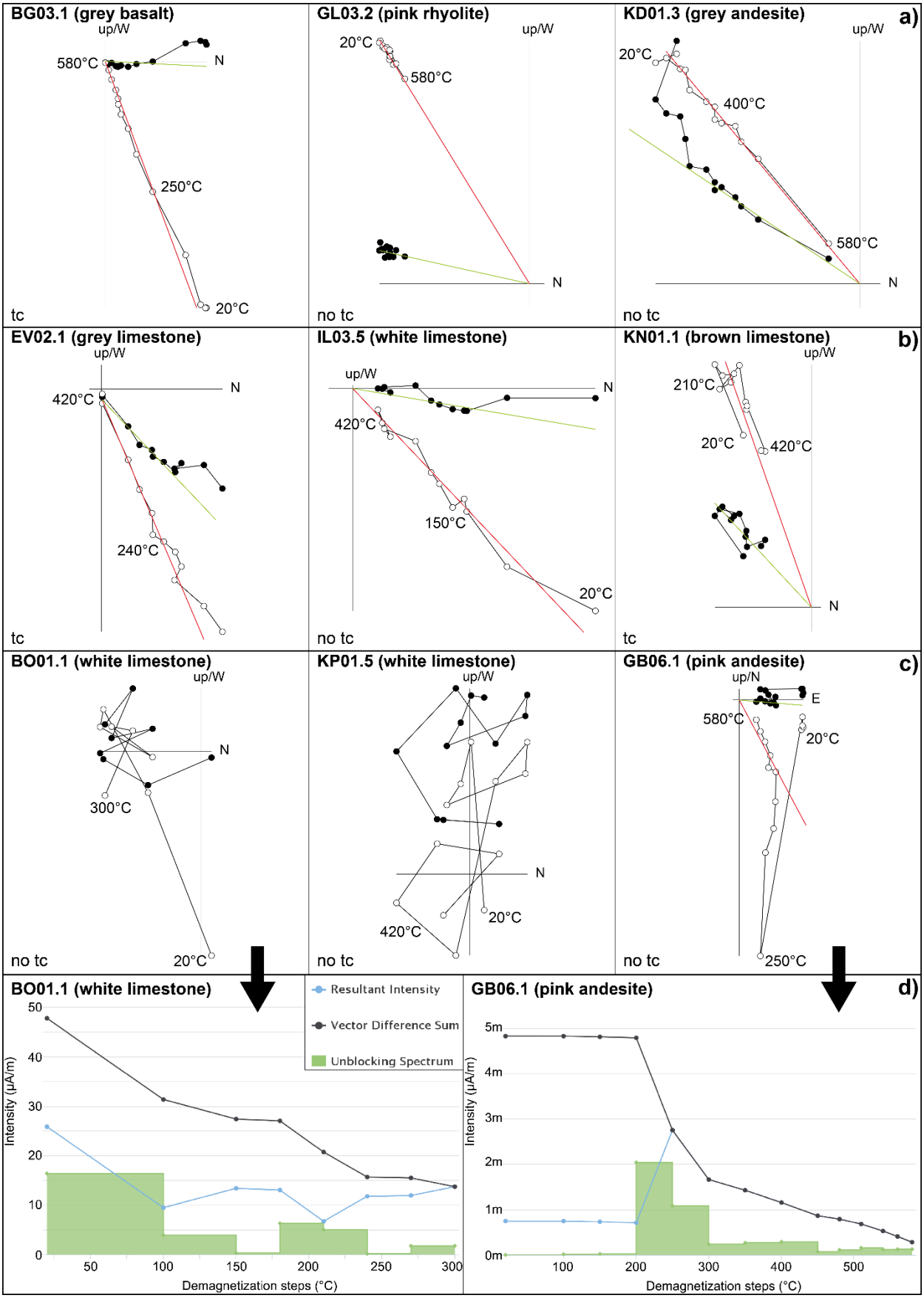


*Fig. 19: Representative volcanic (a) and sedimentary (b) orthogonal vector diagrams (Zijderveld, 1967) from different lithologies in the study area with open/closed dots indicating projections on the vertical/horizontal plane. Tectonic (tc) or geographic (no tc) reference frame is noted per sample, as well as characteristic demagnetization steps. Vertical/horizontal characteristic components are shown in red/green; c) Example specimens from rejected sites are shown in; d) Intensity decay diagrams for BO01.1 and GB06.1. Legend is the same as in figure 17.*

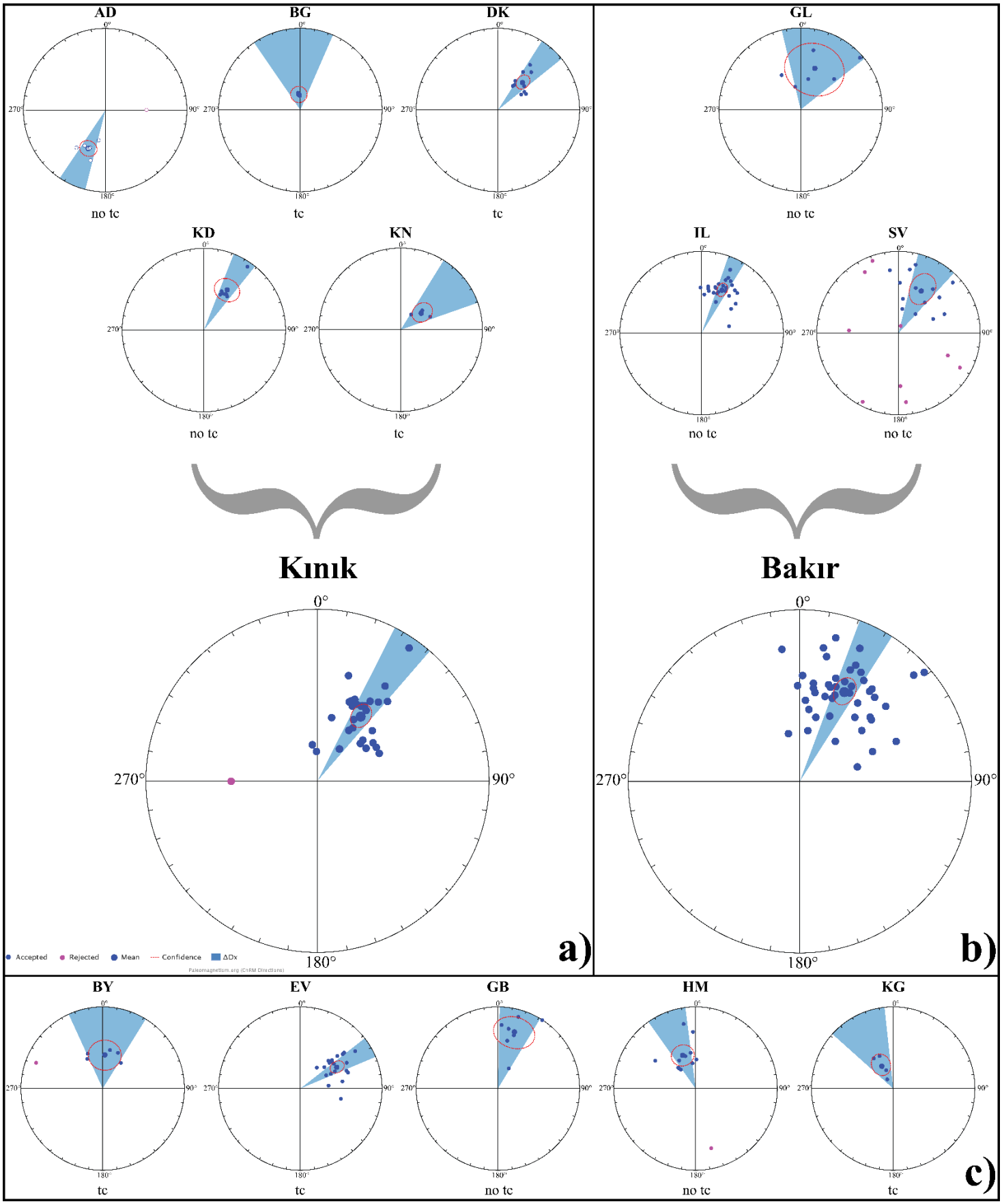


*Fig. 20: Equal area projections of the ChRM directions for all sites from every used locality as well as the resulting tectonic blocks: a) in the south-western quadrant; b) in the eastern quadrant; c) in the northern quadrant. Open/closed symbols indicate projection on upper/lower hemisphere. Blue/pink dots denote used/rejected sites. Mean directions (big blue dots) with their cone of confidence (red dashed line) and $\Delta D_x$ (light blue) are indicated as well. No tc/tc = not corrected/corrected for bedding tilt. Locality abbreviations are listed in figure 4.*

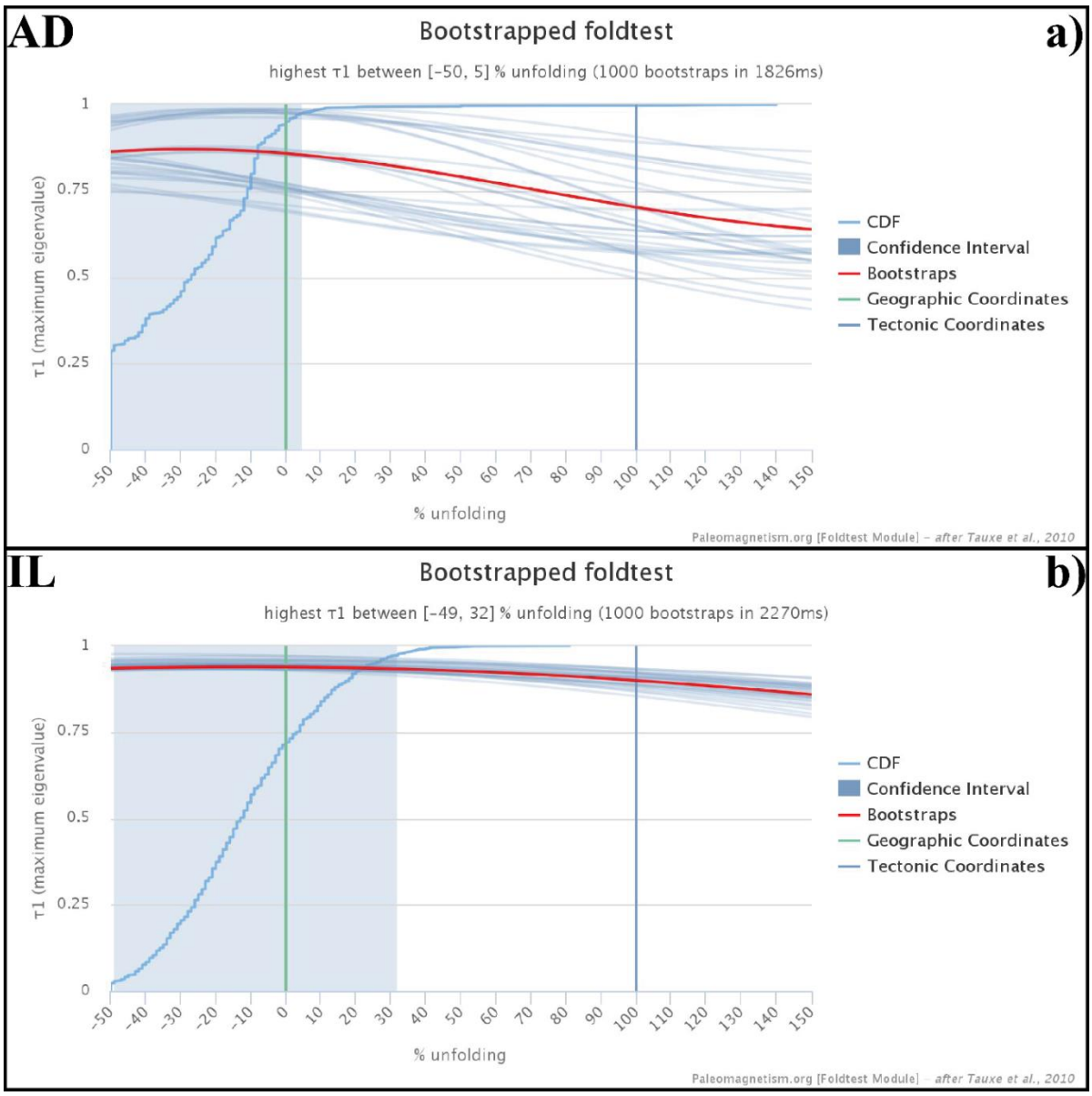


*Fig. 21: Negative fold test from Tauxe & Watson (1994) for: a) volcanic locality Arpadere (AD); b) sedimentary locality Ilyaslar (IL). Legend is indicated on the right.*

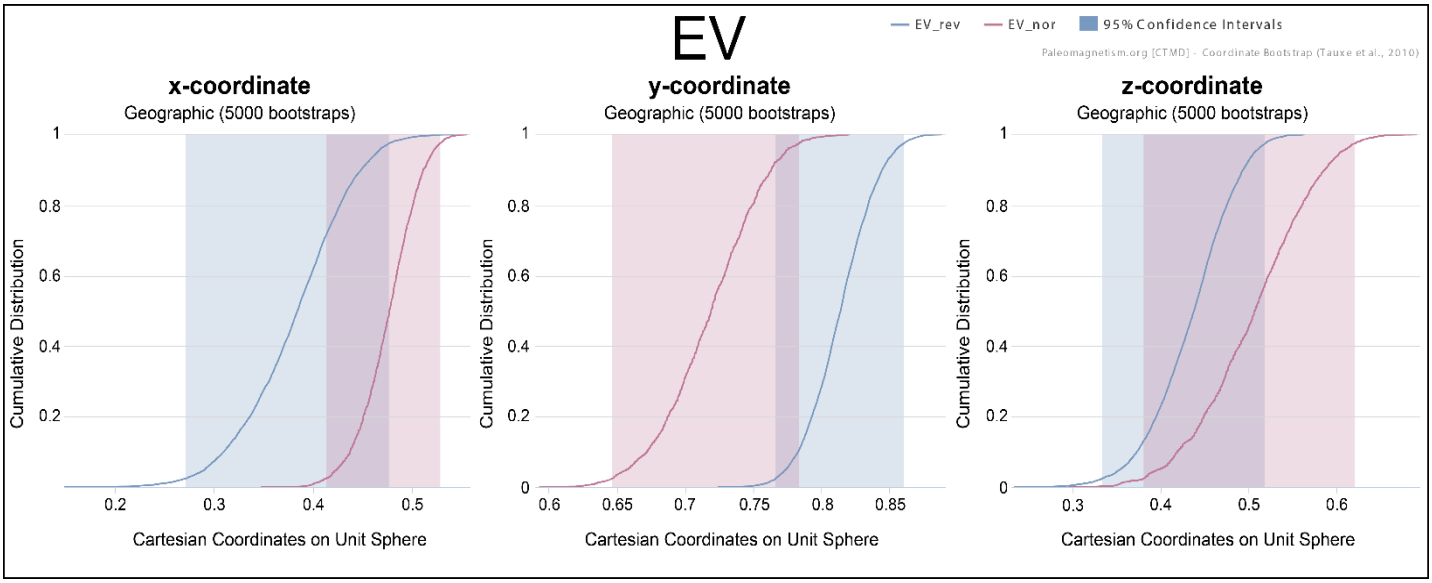


*Fig. 22: Positive reversal test from locality Evciler (EV) using the Cartesian coordinate bootstrap method from Tauxe et al. (2010). The confidence intervals for all three axes overlap. Legend is indicated on the top right.*

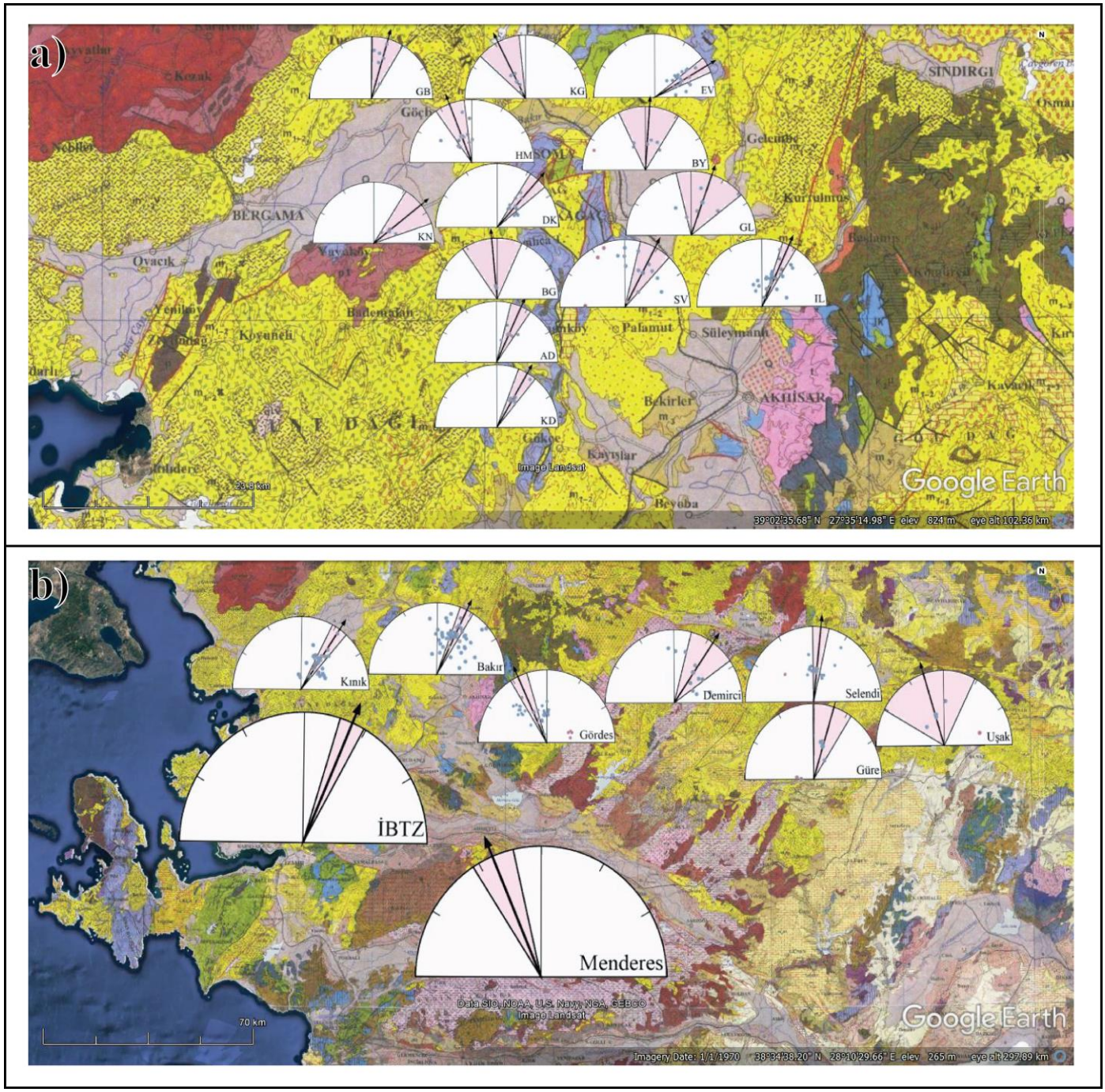


*Fig. 23: a) Resulting Early-Middle Miocene vertical-axis rotations (D and $\Delta D_x$) from this study per locality; b) Vertical-axis rotations in western Anatolia per tectonic block using data from this study (Bakır, Kınık), van Hinsbergen et al. (2010) (Gördes, Demirci, Selendi, Güre, Uşak) and Uzel et al. (2015) (Gördes). The rotations for the whole İBTZ (23.1 ± 6.0°) and Menderes region (337.0 ± 10.2°) from Uzel et al. (2015) are indicated as well. The legend for the geological maps and locality abbreviations are the same as in previous figures (after GDMRE, 2002; Google Earth v. 7.1.5.1557, 39° 7'45.43"N, 27°28'53.60"E, 2016).*

# 5. Discussion

Overall, the paleomagnetic results of this study localities show an average CW net rotation of 29 ± 8° since the Early-Middle Miocene. This is in excellent agreement with previous paleomagnetic results from the İBTZ which yielded an average net rotation of 23 ± 6° *(Uzel et al., 2015, 2016).* In addition, two coherent tectonic blocks with overlapping rotations of 34 ± 7° and 27 ± 6° were constrained in respectively the south-western and eastern quadrant of the Soma basin. Uzel et al. *(2015)* also proposed a system of rigid-block rotations for the whole İBTZ. Therefore, the paleomagnetic results from this study seem to indicate that the Soma basin evolved as part of the İBTZ during the Early-Middle Miocene. However, the northern part of the Soma basin yielded less consistent results. The higher scatter of paleomagnetic directions and generally larger errors in this part of the study area could be related to more abundant deformation in the northern part of the study area, as evidenced by figure 11. Therefore, rigid-block rotation did not take place in the northern part of the Soma basin. This was not foreseen during drilling, as much of the structural geology of the Soma basin was only constrained during this study. The following sections will discuss the detailed deformation history of the Soma basin, as well as how this history can be placed in a regional framework.

## 5.1. Deformation phases

The İBTZ is interpreted as a large-scale NE-SW trending shear zone by recent studies *(Uzel & Sözbilir, 2008; Uzel et al., 2013, 2015).* It is commonly known that such shear zones develop secondary structures during their formation *(Christie-Blick, 1985; Fossen, 2010).* In this context, D1 faults in the Soma basin can be interpreted as synthetic Riedel shears (Fig. 12a), while S1 faults can be interpreted as antithetic Riedel shears (Fig. 13a) based on their general orientations and field observations. Oblique normal components occur in both fault sets. This would indicate that D1 and S1 faults developed simultaneously under NNW-SSE extension and WSW-ENE oriented compression (Fig 13c). The formation of the NNW-SSE oriented F1 folds could be related to these stresses. D1, S1 and F1 structures only deform Early Miocene and older deposits. Therefore, it is likely that they constitute a single transtensional deformation phase, hence called P1, related to the formation of the İBTZ as a wide dextral shear zone during the Early-Middle Miocene. The onset of phase P1 during that time could have triggered volcanism in the area as well, resulting in synchronous deposition of volcanic extrusions and lower sequence sediments, in accordance with the volcanic age results listed in Table 1 from Ersoy et al. *(2014)* and stratigraphic results from this study (Figs. 5, 9c and 16). The bimodal nature of these volcanic extrusions adds further evidence to the transtensional nature of deformation phase P1 *(Till et al., 2007).* The first Miocene deformation phase within the İBTZ from Uzel et al. *(2013)* was also characterized by N-S trending extension and NE-SW trending dextral strike-slip faults. Figure 24a shows a schematic overview of P1. In addition, the CW rotation of rigid tectonic blocks in lower sequence deposits inferred from the paleomagnetic data indicate prevailing dextral shear zone conditions as well *(Christie-Blick, 1985; Uzel, 2013; Waldron, 2001),* as shown in figure 24b. This indicates that the observed vertical-axis rotations from this study are related to P1.
The E-W trending normal faults from fault set N1 cut and displace both D1 faults and F1 folds (Figs. 11 and 16). Furthermore, they deform the Late Miocene-Pliocene Kümkoy formation as well. For these reasons, fault set N1 must be related to a younger deformation phase than P1. This younger deformation phase is hence called P2. It was most likely transtensional due to the large oblique components of N1 faults (Fig 12a) and the occurrence

of the NE-SW trending GFZ, which is still active at present *(İnan et al., 2012).* According to figure 14, N1 faults must have formed under a generally N-S trending extensional regime. However, the normal faults often have large oblique components and slip directions are more variable compared to D1 faults. Reactivation of older faults could be an explanation for this. Uzel *(2016)* also found evidence for reactivation of the large-scale Bakır and Kirkağaç faults. Indeed, the NW-SE trending orientations of both faults correspond to S1 faults from deformation phase P1, while their slip directions correspond to normal faulting (Table 4). Overall, these results correspond to the last deformation phase from Uzel et al. *(2013)* which was also characterized by E-W trending normal faults during the Late Miocene-Pliocene. Furthermore, Uzel et al. *(2013, 2015)* suggested that the İBTZ evolved in a narrower fault zone where strike-slip and extensional deformation were completely decoupled during this final deformation phase. In the Soma basin, this can be inferred from the occurrence of the undisturbed and large-scale GFZ alongside the N1 normal faults.

In this context, the only unresolved structures within the Soma basin are the F2 folds. They are incompatible with the P1 principal stresses (Fig. 12c). Furthermore, they deform the Kümkoy formation as well. Therefore, they could be related to a third deformation phase. Uzel et al. *(2013)* also found evidence for the occurrence of a third deformation phase within the İBTZ. However, no corresponding faults have been observed in the Soma basin to prove this. Another explanation is that F2 folds are related to local stress changes during phase P2, possibly related to differences in fault offsets or local-block rotations, resulting in oblique extensional N1 faults. It is not uncommon for folds to develop in a transtensional setting *(Janecke et al., 1998).* Furthermore, Sözbilir *(2002)* found evidence for the occurrence of such transtensional folds in the nearby Gediz basin. Figure 24c shows a schematic drawing for phase P2 in this context. This interpretation nicely explains the orientation of the GFZ as well.

Therefore, the results from this study indicate that the Soma basin underwent multiple transtensional deformation phases in accordance with the prevailing ideas about the İBTZ and western Anatolia as a whole (*Beccaletto & Steiner, 2005; Bozkurt, 2001; Bozkurt & Sözbilir, 2004, 2006; Bozkurt & Mittwede, 2005; Emre & Sözbilir 2007; Kaya et al., 2004, 2007; Kaymakci 2006; Koçyiğit et al., 1999; Purvis & Robertson 2004, 2005; Sözbilir, 2001; Uzel et al., 2013; Uzel et al., 2015; Yılmaz et al., 2000)*. N-S trending extension was dominant in the Soma basin throughout P1 and P2. This can also be inferred from the AMS data of this study (Figs. 18 and 24). Only the second CCW rotational phase from Uzel et al. *(2015)* within the İBTZ is not accounted for in this study. This can be attributed to the absence of reliable results from the two upper sequence localities (Beyoba and Kapaklı). The only locality that does show a consistent CCW rotation is Hamidiye. However, this locality should be Early Miocene in age according geological field cross-section B-B' (Fig. 16). Therefore, the differing rotation from Hamidiye compared to other lower sequence localities could be related to its proximity to a large strike-slip fault which likely represents the reactivated IAS suture, resulting in local-block rotation.

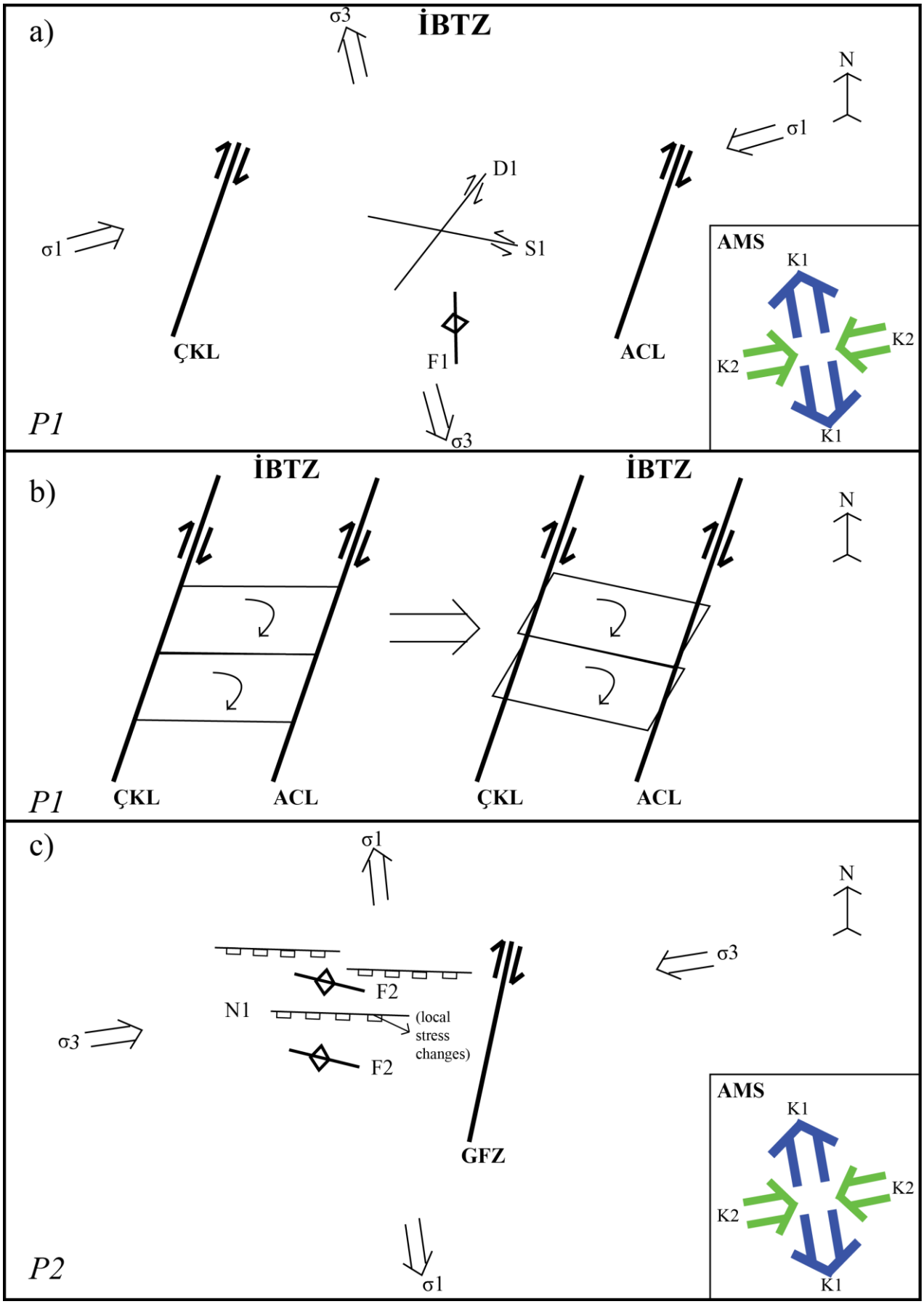


*Fig. 24: a) Schematic overview of deformation phase P1. All structures related to this deformation phase are drawn (D1 = dextral strike-slip fault set 1, S1 = sinistral strike-slip fault set 1, F1 = fold set 1), as well as the principal stress directions $\sigma_1$ and $\sigma_3$. ACL = Appak–Cumaovası Lineament, ÇKL = Çandarlı–Karaburun Lineament (from Uzel et al., 2015); b) Schematic drawing of tectonic block rotations as a result of dextral strike-slip faulting in the İBTZ during P1; c) Schematic overview of deformation phase P2. GFZ = Gelenbe Fault Zone. The AMS results from figure 18 are indicated as well for comparison.*

## 5.2. Regional implications

Throughout deformation phases P1 and P2, particularly in the GFZ in the latter, strike-slip deformation was dominant in the Soma basin. Structural and AMS results also provided evidence for N-S trending extension during these two phases. There was a basin-and-range type of structural style according to the geological field cross-sections (Fig. 16). For these reasons, the Soma basin can be interpreted as a pull-apart basin. Formation of the basin was superimposed on pre-existing structures related to an Alpine active margin phase, as evidenced by the IAS (Fig. 11), in accordance with Kaya *(1981)*. Furthermore, observations from this study indicate that the transtensional deformation evolved from a wide shear zone (P1) into a narrow strike-slip fault zone, where extensional and strike-slip fault faulting were effectively decoupled from each other (P2). Uzel et al. *(2013, 2015)* observed this in other parts of the İBTZ as well and related it to strain softening *(Naylor et al., 1986)* at higher strain rates caused by heat generated from the Miocene volcanism. Therefore, the evolution of the Soma basin agrees with the formation of other Neogene basins within the İBTZ *(Uzel & Sozbilir, 2008; Uzel et al., 2013; Uzel et al., 2015)*. However, while the presence of the MMU can be identified in other basins within the İBTZ *(Uzel et al., 2015, 2016)*, it cannot be directly observed in the Soma basin. This is likely caused by the lack of stratigraphic observations in upper sequence outcrops and the absence of reliable upper sequence paleomagnetic data, as its presence can be inferred from the timing of P1. The paleomagnetic results from this study are in excellent agreement with the rest of the İBTZ *(Uzel et al., 2015)*, as discussed before. The deformation phases observed in the Soma basin correspond with the results of Uzel et al. *(2013)*, with the exception of their second deformation phase. Therefore, it can be stated that the İBTZ system as identified by previous studies *(Ring et al., 1999; Sözbilir et al., 2011; Uzel and Sözbilir, 2008; Uzel et al., 2013, 2015, 2016)*, continues northward up until the northern part of the Soma basin without influences of the NAFZ. The intense faulting and incoherent rotations in the northern part of the basin are an indication for disturbance of the system which could be the NAFZ. Future research of the area will provide more insight in this matter.

In addition to this, the two transtensional deformation phases constrained by this study fit into the two-stage Neogene extension hypothesis for the whole Aegean region from Brun et al. *(2016)*. This hypothesis suggests that there was a sharp transition from localized extension during the first Early-Middle Miocene stage to distributed extension during the second Late Miocene-Pliocene stage. This could have been caused by an increase in strain rate *(Brun, 1999; Schueller et al. 2005, 2010)* which is also inferred from the narrowing of the İBTZ between P1 and P2. Brun et al. *(2016)* related this increase in strain rate to an acceleration of slab rollback of the Aegean slab. Therefore, the two deformation phases in the Soma basin as part of the İBTZ, as constrained by this study, add further credibility to the hypothesis that rollback of the Aegean slab (Fig. 1) is the primary cause for western Anatolian tectonics during the Neogene.

The remaining question is how the single-phase asymmetrical exhumation of the MCC from van Hinsbergen et al. *(2010)* can be fitted with two-stage Neogene extension in western Anatolia and the occurrence of the İBTZ. To answer this question, the data from van Hinsbergen et al. *(2010)* of the NMM-basins, directly east of the Soma basin, were reinterpreted and separated per basin. Furthermore, their data for the Gördes basin was merged with the results from Uzel et al. *(2015)*. Finally, the age of all sampled localities was checked, verifying that the vertical-axis rotations are Early-Middle Miocene in age. The revisited data for all NMM-basins (Gördes, Demirci, Selindi, Güre, Uşak and Ahmetlar) are listed in Table 6 and shown in figure 23b, alongside the results from this study. Van Hinsbergen et al. *(2010)* found a CW rotation of 13 ± 9° for the combined NMM-basins.


*Fig. 25: Schematic representation of western Anatolian tectonics during the first Early-Middle Miocene deformation phase. The study area of this research is indicated in pink. Rotational trends for different tectonic blocks are drawn in purple, using the results from (1) van Hinsbergen et al. (2010), (2) Uzel et al. (2015), (3) this study. Principal stress directions are indicated with black arrows. Major fault systems are drawn as well, where ACL = Appak–Cumaovası Lineament, AD = Alaşehir Detachment, ÇKL = Çandarlı–Karaburun Lineament, GG = Gediz Graben, KMG = Küçük Menderes Graben, SD = Simav detachment, SG = Simav Graben. AD defines a pivot line, separating CW rotation in the northern Menderes region from CCW rotation in the southern Menderes region and Lycian Nappes. The legend for the geological map is the same as in previous figures (after GDMRE, 2002).*

Table 6 still indicates a dominantly CW rotation for most NMM-basins (Demirci, Selindi, Güre). Ahmetlar and Uşak did not yield reliable results, while Gördes displays a CCW rotation of 26 ± 8°. According to Şengör *(1987)*, it should be possible for the NMM-basins to exhibit small differences in vertical-axis rotations due to the cross-faults bordering them. For these reasons, the interpretation of van Hinsbergen et al. *(2010)*, where the AD acts as a pivot line and separates CW rotation in the northern Menderes region from CCW rotation in the southern part and in the Lycian Nappes resulting from asymmetrical exhumation of the MCC, remains well-argued, because both Uzel et al. *(2015)* and van Hinsbergen et al. *(2010)* found CCW rotations for the area south of the AD. It seems likely that this extensional system was interrupted in the west by a differential amount of extension in the CCC, resulting in the development of the İBTZ as a wide shear zone in the Early-Middle Miocene. This is all in accordance with the interpretation of Uzel et al. *(2013, 2015)* and deformation phase P1 from this study (Fig. 24). In this context, CCW rotation in the Gördes basin could have accommodated extensional exhumation in the Menderes region and strike-slip deformation in the Soma basin as part of the İBTZ. It should be noted that the Gördes basin is bordered in the east and west by dextral strike-slip faults *(Şengör, 1987)* which would normally result in CW rotation instead of CCW *(Christie-blick, 1985; Waldron, 2001)*. However, fault displacements in the large-scale İBTZ west of Gördes are most likely more substantial than in

the smaller-scale cross-faults east of Gördes. Therefore, the Gördes basin likely underwent CCW rotation due to the dominant influence of İBTZ system. The resulting interpretation for the whole region during the first Early-Middle Miocene deformation phase is shown in figure 25. After this first phase, the regional configuration was replaced by the Late Miocene-Pliocene distributed extensional system *(Brun et al., 2016; Uzel et al., 2015)*, which was described before.

# 6. Conclusions

New paleomagnetic, AMS, stratigraphic and structural data from the Soma basin show that it evolved as a pull-apart basin as part of the İBTZ during at least two deformation phases in the Neogene. According to the structural and AMS results, deformation was dominated by NE-SW trending dextral strike-slip faulting related to approximately N-S trending extension during both phases. During the first Early-Middle Miocene deformation phase, the Soma basin was part of a large-scale dextral shear zone consisting of at least two rigid tectonic blocks with an average CW net rotation of 29 ± 8°, as evidenced by the paleomagnetic vertical-axis rotations. In the second Late Miocene-Pliocene deformation phase, the distribution of NE-SW trending dextral strike-slip faulting narrowed and was decoupled from E-W trending normal faulting. These results are in excellent agreement with the rest of the İBTZ, indicating that it continues northward up until at least the northern part of the Soma basin. In the northern part, the presence of incoherent rotations and more intense deformation are an indication of disturbance of this system, possibly by the nearby NAFZ. In this context, the results from this study show that the İBTZ effectively accommodated asymmetric extensional exhumation of the MCC and a differential amount of extension in the CCC during the first deformation phase. After that, the mode of extension in western Anatolia changed from localized to distributed, related to slab-tearing of the Aegean slab and subsequent acceleration of rollback. Therefore, the results from this study add further credibility to the prevailing ideas about the whole Aegean region.

# Acknowledgements

First of all, I would like to thank my two supervisors, Cor Langereis and Bora Uzel. Both of them were always helpful, trustful and enthusiastic. Supervision sessions with Cor were interesting and fun. He invested a lot of time in me despite his busy schedule, like the one time we spend two days figuring out how a very weird piece of software worked. Bora's attitude and knowledge in the field really motivated me to get the best out of myself during two great fieldtrips in Turkey (Hadi gari!). Back in Holland, he never hesitated to answer my mails about literature and structural data.
In addition to them, teşekkürler Nuretdin Kaymakci, Emre Kırhan and İsmail Duran for the good times in Turkey and their help/knowledge in the field. And of course for enabling communication with the locals. I would to thank Nuri for helping me with checking my interpretations and first version as well.
Furthermore, I would like to thank Jorik Poessé and Thomas van der Werf for their constructive remarks on my first version.
Last but not least, many thanks to everybody from Fort Hoofddijk for their friendliness and especially Lennart de Groot, Annique van der Boon, Dan Palcu, Maxim Krasnoperov and Annemarieke Béguin for helping to explain how all the machines and corresponding software in the Fort worked.

# References


- Akdeniz, N., & Tetkik, M. (1980). Başlamış formasyonu. Jeoloji Mühendisliği, 10, 39-47.
- Akgün, F., Kayseri, M. S., & Akkiraz, M. S. (2007). Palaeoclimatic evolution and vegetational changes during the Late Oligocene–Miocene period in Western and Central Anatolia (Turkey). Palaeogeography, Palaeoclimatology, Palaeoecology, 253(1), 56-90.
- Akkök, R. (1983). Structural and metamorphic evolution of the Menderes Massif: new data from the Derbent area and their implication for the tectonics of the massif. Journal of Geology 91, 342–350.
- Aktuğ, B. & Kılıçoğlu, A. (2006). Recent crustal deformation of İzmir, western Anatolia and surrounding regions as deduced from repeated GPS measurements and strain field. Journal of Geodynamics, 41, 471–484.
- Aldanmaz, E., Pearce, J. A., Thirlwall, M. F., & Mitchell, J. G. (2000). Petrogenetic evolution of late Cenozoic, post-collision volcanism in western Anatolia, Turkey. Journal of Volcanology and Geothermal Research, 102(1), 67-95.
- Altunkaynak, Ş., Rogers, N. W., & Kelley, S. P. (2010). Causes and effects of geochemical variations in late Cenozoic volcanism of the Foça volcanic centre, NW Anatolia, Turkey. International Geology Review, 52(4-6), 579-607.
- Beccaletto, L., & Steiner, C. (2005). Evidence of two-stage extensional tectonics from the northern edge of the Edremit Graben, NW Turkey. Geodinamica Acta, 18(3-4), 283-297.
- Biryol, C. B., Beck, S. L., Zandt, G., & Özacar, A. A. (2011). Segmented African lithosphere beneath the Anatolian region inferred from teleseismic P-wave tomography. Geophysical Journal International, 184(3), 1037-1057.
- Bozkurt, E. & Park, R.G. (1997). Microstructures of deformed grains in the augen gneisses of southern Menderes massif and their tectonic significance, western Turkey. Geologische Rundschau, 86, 101–119.
- Bozkurt, E. (2000). Timing of extension on the Büyük Menderes Graben, western Turkey, and its tectonic implications, in Tectonics and Magmatism in Turkey and the Surrounding Area, E. Bozkurt et al. (Eds.). Geol. Soc. Spec. Publ., 173, 385–403, doi:10.1144/GSL.SP.2000.173.01.18.
- Bozkurt, E., 2001. Neotectonics of Turkey—a synthesis. Geodin. Acta14, 3–30.
- Bozkurt, E., & Mittwede, S. K. (2001). Introduction to the geology of Turkey—a synthesis. International Geology Review, 43(7), 578-594. ISO 690.
- Bozkurt, E. & Sözbilir, H. (2004). Tectonic evolution of the Gediz Graben: field evidence for an episodic, two extension in western Turkey. Geological Magazine, 141, 63–79.
- Bozkurt, E. & Mittwede, S.K. (2005). Introduction: evolution of Neogene extensional tectonics of western Turkey. Geodinamica Acta, 18, 153–165.
- Bozkurt, E. & Sözbilir, H. (2006). Evolution of the large-scale active Manisa Fault, southwest Turkey: Implications on fault development and regional tectonics. Geodinamica Acta, 19, 427−453.
- Brun, J. P. (1999). Narrow rifts versus wide rifts: inferences for the mechanics of rifting from laboratory experiments. Philosophical Transactions-Royal Society of London Series A Mathematical Physical and Engineering Sciences, 695-709.

- Brun, J., Faccenna, C., Gueydan, F., Sokoutis, D., Philippon, M., Kydonakis, K., Gorini, C. (2016). The two-stage Aegean extension, from localized to distributed, a result of slab rollback acceleration. Canadian Journal of Earth Sciences. cjes-2015-0203.R1.
- Butler, R.F. (1992). Paleomagnetism: Magnetic Domains to Geologic Terranes. Black-well Publishing, Boston. 195 pp.
- Candan, O., Dora, O.Ö., Oberhansli, R., Oelsner, F., Durr, S. (1997). Blueschist relics in the Mesozoic cover series of the Menderes Massif and correlations with Samos Island, Cyclades. Schweizerische Mineralogische Und Petrographische Mitteilungen 77, 95–99.
- Candan, O., Dora, O.Ö., Oberhansli, R., Çetinkaplan, M., Partzsch, J.H., Warkus, F.C., Durr, S. (2001). Pan-African high-pressure metamorphism in the Precambrian basement of the Menderes Massif, Western Anatolia, Turkey. International Journal of Earth Science 89, 793–811.
- Christie-Blick, N. (1985). Deformation and basin formation along strike-slip faults.
- Çiftçi, N. B., & E. Bozkurt (2009). Evolution of the Miocene sedimentary fill of the Gediz Graben, SW Turkey, Sedimentary Geology, 216, 49–79, doi:10.1016/j. sedgeo.2009.01.004.
- Dankers, P. H. M. (1978). Magnetic properties of dispersed natural iron-oxides of known grain size. ISO 690
- Deenen, M.H.L., Langereis, C.G., van Hinsbergen, D.J.J., Biggin, A.J. (2011). Geomagnetic secular variation and the statistics of palaeomagnetic directions. Geophys. J. Int.186, 509–520.
- Deenen, M.H.L., Langereis, C.G., van Hinsbergen, D.J.J., Biggin, A.J. (2014). Erratum to: Geomagnetic secular variation and the statistics of palaeomagnetic directions [Geophys. J. Int. 186 (2011) 509–520]. Geophys. J. Int.197, 643.
- Delvaux, D., & Sperner, B. (2003). New aspects of tectonic stress inversion with reference to the TENSOR program. Geological Society, London, Special Publications, 212(1), 75-100.
- Delvaux, D. and Sperner, B. (2003). Stress tensor inversion from fault kinematic indicators and focal mechanism data: the TENSOR program. In: New Insights into Structural Interpretation and Modelling (D. Nieuwland Ed.). Geological Society, London, Special Publications, 212: 75-100.
- Dewey, J.F., Hempton, M.R., Kidd, W. S.F., Şaroğlu, F. & Şengör, A.M.C. (1986). Shortening of Continental Lithosphere: The Neotectonics of Eastern Anatolia-A Young Collision Zone. Geological Society Special Publication, 19, 3−37.
- Dunlop, D.J., Özdemir, Ö. (1997). Rock Magnetism - Fundamentals and Frontiers.
- Ercan, E., Satır, M., Sevin, D., Türkecan, A. (1996). Batı Anadolu'daki Tersiyer ve Kuvaterner yaşlı volkanik kayaçlarda yeni yapılan radyometrik yaş ölçümlerinin yorumu [Some new radiometric ages from Tertiary and Quaternary volcanic rocks from West Anatolia]. Miner. Res. Explor. Bull. (Turkey) 119, 103–112.
- Emre, T., & Sözbilir, H. (2007). Tectonic evolution of the Kiraz Basin, Küçük Menderes Graben: evidence for compression/uplift-related basin formation overprinted by extensional tectonics in West Anatolia. Turkish Journal of Earth Sciences, 16(4), 441-470.
- Erdoğan, B. (1990). Tectonic relations between İzmir–Ankara Zone and Karaburun Belt. Bulletin of Mineral Research and Exploration Institute of Turkey, 110, 1–15.

- Erkül, F., Helvacı, C., Sözbilir, H. (2005). Stratigraphy and geochronology of the Early Miocene volcanic units in the Bigadiç Borate Basin, Western Turkey. Turk. J. Earth Sci. 14, 227–253.
- Ersoy, E. Y., Çemen, İ., Helvacı, C., & Billor, Z. (2014). Tectono-stratigraphy of the Neogene basins in Western Turkey: Implications for tectonic evolution of the Aegean Extended Region. Tectonophysics, 635, 33-58.
- Fisher, R.A. (1953). Dispersion on a sphere. Proceedings of the Royal Society of London, Series A, 217, 295–305, doi:10.1098/rspa.1953.0064.
- Fossen, H. (2010). Structural geology. Cambridge: Cambridge University Press (463 p.).
- Genç, Ş. C., & Tüysüz, O. (2010). Tectonic setting of the Jurassic bimodal magmatism in the Sakarya Zone (Central and Western Pontides), Northern Turkey: a geochemical and isotopic approach. Lithos, 118(1), 95-111.
- General Directorate of Mineral Resarch and Exploration (GDMRE) (2002). Geological map of the Turkey. Map section of study area, Yuntdağ.
- Gessner, K., Gallardo, L. A., Markwitz, V., Ring, U., & Thomson, S. N. (2013). What caused the denudation of the Menderes Massif: Review of crustal evolution, lithosphere structure, and dynamic topography in southwest Turkey. Gondwana Research, 24(1), 243-274.
- Google Inc. (2009). Google Earth (Version 7.1.5.1557). Available from: https://www.google.nl/intl/nl/earth/.
- Govers, R., & Wortel, M. J. R. (2005). Lithosphere tearing at STEP faults: response to edges of subduction zones. Earth and Planetary Science Letters, 236(1), 505-523.
- Hopkinson, J. (1889). Magnetic and other physical properties of iron at a high temperature. Philosophical Transactions of the Royal Society of London. A, 180, 443-465.
- Hrouda, F. (1982). Magnetic anisotropy of rocks and its application in geology and geophysics. Geophysical surveys, 5(1), 37-82.
- İnan, S., Pabuçcu, Z., Kulak, F., Ergintav, S., Tatar, O., Altunel, E., ... & Saatçılar, R. (2012). Microplate boundaries as obstacles to pre-earthquake strain transfer in Western Turkey: inferences from continuous geochemical monitoring. Journal of Asian Earth Sciences, 48, 56-71.
- İncı, U. (1998). Lignite and carbonate deposition in Middle Lignite succession of the Soma Formation, Soma coalfield, western Turkey. International Journal of Coal Geology, 37(3), 287-313.
- İncı, U., 2002. Depositional evolution of Miocene coal successions in the Soma coalfield, western Turkey. Int. J. Coal Geol. 51, 1–29.
- İncı, U., Koçyiğit, A., Bozkurt, E., Arpalıyiğit, İ., (2003) BİRİMLERİ, P. K. SOMA VE KIRKAĞAÇ GRABENLERİNİN KUVATERNER JEOLOJİSİ, BATI ANADOLU. İTÜ Avrasya Yerbilimleri.
- Innocenti, F., Agostini, S., Di Vincenzo, G., Doglioni, C., Manetti, P., Savaşçın, M.Y., Tonarini, S. (2005). Neogene and Quaternary volcanism in Western Anatolia: magma sources and geodynamic evolution. Mar. Geol. 221, 397–421.
- Janecke, S. U., Vandenburg, C. J., & Blankenau, J. J. (1998). Geometry, mechanisms and significance of extensional folds from examples in the Rocky Mountain Basin and Range province, USA. Journal of Structural Geology, 20(7), 841-856
- Jelinek, V., & Kropáček, R. V. (1978). Statistical processing of anisotropy of magnetic susceptibility measured on groups of specimens. Studia geophysica et geodaetica, 22(1), 50-62.

- Jelinek, V. (1981). Characterization of the magnetic fabric of rocks. Tectonophysics, 79(3-4), T63-T67.
- Jolivet, J., Rimmelé, G., Oberhänsli, R., Goffé, B. & Candan, O. (2004). Correlation of syn- orogenic tectonic and metamorphic events in the Cyclades, the Lycian Nappes and the Menderes Massif. Geodynamic implications. Bulletin de la Société Géologique de France, 175, 217–238.
- Jolivet, L. & Brun, J.P. (2010). Cenozoic geodynamic evolution of the Aegean. International Journal of Earth Sciences, 99, 109–138.
- Jolivet, L., Faccenna, C., Huet, B., Labrousse, L., Le Pourhiet, L., Lacombe, O., ... & Philippon, M. (2013). Aegean tectonics: Strain localisation, slab tearing and trench retreat. Tectonophysics, 597, 1-33.
- Kaya, O. (1981). Miocene reference section for the coastal parts of West Anatolia. Newsl. Stratigr.10, 164–191.
- Kaya, O., Ünay, E., Saraç, G., Eichhorn, S., Hassenrück, S., Knappe, A., ... & Mayda, S. (2004). Halitpaşa transpressive zone: implications for an Early Pliocene compressional phase in central western Anatolia, Turkey. Turkish Journal of Earth Sciences, 13(1), 1-13.
- Kaya, O., Ünay, E., Göktaş, F. & Saraç G. (2007). Early Miocene stratigraphy of central west Anatolia, Turkey: Implications for the tectonic evolution of the eastern Aegean area, Geological Journal, 42, 85–109, doi:10.1002/gj.1071.
- Kaymakci, N. (2006). Kinematic development and paleostress analysis of Denizli basin (w Turkey): implications of spatial variation of relative paleostress magnitudes and orientations. J Asian Earth Sci, 27, 207222.
- Kaymakci, N., Aldanmaz, E., Langereis, C., Spell, T. L., Gurer, O. F., & Zanetti, K. A. (2007). Late Miocene transcurrent tectonics in NW Turkey: evidence from palaeomagnetism and 40Ar-39Ar dating of alkaline volcanic rocks. Geological Magazine, 144(2), 379.
- Kirschvink, J.L. (1980). The least-squares line and plane and the analysis of paleomagnetic data. Geophysical Journal of the Royal Astronomical Society, 62, 699–718.
- Kissel, C., Poisson, A. (1987). Étude paléomagnetique préliminaire des formations cénozoïques des Bey Daglari (Taurides occidentales, Turquie). C. R. Acad. Sci. Ser. II304 (8), 343–348.
- KOÇYIĐIT, A., YUSUFOĐLU, H., & BOZKURT, E. (1999). Evidence from the Gediz graben for episodic two-stage extension in western Turkey. Journal of the Geological Society, 156(3), 605-616.
- KOÇYİĞİT, A., & Özacar, A. A. (2003). Extensional neotectonic regime through the NE edge of the Outer Isparta Angle, SW Turkey: new field and seismic data. Turkish Journal of Earth Sciences, 12(1), 67-90.
- Kondopoulou, D., Sen, S., Aidona, E., Van Hinsbergen, D. J. J., & Koufos, G. (2011). Rotation history of Chios island, Greece since the Middle Miocene. Journal of Geodynamics, 51(5), 327-338.
- Koymans, M. R., Langereis, C. G., Pastor-Galán, D., & van Hinsbergen, D. J. (2016). Paleomagnetism. org: an online multi-platform open source environment for paleomagnetic data analysis. Computers & Geosciences, 93, 127-137.
- Le Pichon, X. & Angelier J. (1979). The Hellenic arc and trench system: A key to the neotectonic evolution of the eastern Mediterranean area. Tectonophysics, 60, 1–42.

- McFadden, P.L., McElhinny, M.W. (1988). The combined analysis of remagnetisation circles and direct observations in paleomagnetism. Earth Planet. Sci. Lett.87, 161–172.
- Meulenkamp, J.E., Wortel, M.J.R., van Wamel, W.A., Spakman, W. & Hoogerduyn Strating E. (1988). On the Hellenic subduction zone and the geodynamical evolution of Crete since the late middle Miocene. Tectonophysics, 146, 203–215.
- Morris, A., Anderson, M. (1996). First palaeomagnetic results from the Cycladic Massif, Greece, and their implications for Miocene extension directions and tectonic models in the Aegean. Earth and Planetary Science Letters, 142, 397–408.
- Mullender, T.A.T., van Velzen, A.J., Dekkers, M.J. (1993). Continuous drift correction and separate identification of ferrimagnetic and paramagnetic contribution in thermomagnetic runs. Geophys. J. Int.114, 663–672.
- Naylor, M.A., Mandl, G., Sijpesteijn, C.H.K. (1986). Fault geometries in basement-induced wrench faulting under different initial stress states. J. Struct. Geol.8, 737–752.
- NEBERT, K. (1978). Linyit iceren Soma Neojen bölgesi, Bati Anadolu. Mineral Research and Exploration Institute of Turkey (MTA) Bulletin, 90, 20-69.
- Okay, A.İ. & Siyako, M. (1993). The new position of the İzmir-Ankara Neo-Tethyan Suture between İzmir and Balıkesir. Proceedings of the Ozan Sungurlu Symposium, pp. 333–355.
- Okay, A.İ. (2001). Stratigraphic and metamorphic inversions in the central Menderes Massif: A new structural model. Int. J. Earth Science, 89, 709–727, doi:10.1007/s005310000098.
- Okay, A. I., İşintek, İ., Altıner, D., Özkan-Altıner, S., & Okay, N. (2012). An olistostrome–mélange belt formed along a suture: Bornova Flysch zone, western Turkey. Tectonophysics, 568, 282-295.
- Paul, A., Karabulut, H., Mutlu, A. K., & Salaün, G. (2014). A comprehensive and densely sampled map of shear-wave azimuthal anisotropy in the Aegean–Anatolia region. Earth and Planetary Science Letters, 389, 14-22.
- Pe-Piper, G., Piper, D.J.W. & Matarangas, D. (2002). Regional implications of geochemistry and style of emplacement of Miocene I-type diorite and granite, Delos, Cyclades, Greece. Lithos, 60, 47–66.
- Philippon, M., Brun, J.P. & Gueydan, F. (2012). Deciphering subduction from exhumation in the segmented Cycladic Blueschist Unit (Central Aegean, Greece). Tectonophysics, 524–525, 116–134. http://dx.doi.org/10.1016/j.tecto.2011.12.025.
- Philippon, M., Brun, J.P., Gueydan, F. & Sokoutis, D. (2014). The interaction between Aegean back-arc extension and Anatolia escape since Middle Miocene. Tectonophysics, 631, 176–188. doi:10.1016/j.tecto.2014.04.039.
- Pickett, E. A., & Robertson, A. H. (1996). Formation of the Late Palaeozoic–Early Mesozoic Karakaya Complex and related ophiolites in NW Turkey by Palaeotethyan subduction–accretion. Journal of the Geological Society, 153(6), 995-1009.
- Purvis, M., Robertson, A. (2004). A pulsed extension model for the Neogene-Recent E–W-trending Alas¸ ehir Graben and the NE–SW-trending Selendi and Gördes Basins, Western Turkey. Tectonophysics, 391, 171–201.
- Purvis, M., Robertson, A.H.F. (2005). Sedimentation of the Neogene–Recent Alaşehir (Gediz) continental graben system used to test alternative tectonic models for western (Aegean) Turkey. Sedimentary Geology, 173, 373–408.

- Ring, U., Susanne, L. & Matthias, B. (1999). Structural analysis of a complex nappe sequence and late orogenic basins from the Aegean Island of Samos, Greece. Journal of Structural Geology, 21, 1575–1601.
- Sarı, B. (2012). Late Maastrichtian–Late Palaeocene planktic foraminiferal biostratigraphy of the matrix of the Bornova Flysch Zone around Bornova. Turkish Journal of Earth Sciences (in press), doi:10.3906/yer-1107-2.
- Schueller, S., Gueydan, F., & Davy, P. (2005). Brittle-ductile coupling: Role of ductile viscosity on brittle fracturing. Geophysical Research Letters, 32(10).
- Schueller, S., Gueydan, F., & Davy, P. (2010). Mechanics of the transition from localized to distributed fracturing in layered brittle–ductile systems. Tectonophysics, 484(1), 48-59.
- Şen, S., Seyitoğlu, G. (2009). Magnetostratigraphy of early–middle Miocene deposits from east–west trending Alaşehir and Büyük Menderes grabens in western Turkey, and its tectonic implications. In: van Hinsbergen, D.J.J., et al. (Eds.), Collision and Collapse at the Africa–Arabia–Eurasia Subduction Zone. In: Geol. Soc. (Lond.) Spec. Publ., vol.311, pp.321–342.
- Şengör, A.M.C. (1979). The North Anatolian Transform Fault: its age, offset and tectonic significance. Journal of the Geological Society of London, 136, 269–282.
- Şengör, A.M.C. & Yılmaz, Y. (1981). Tethyan evolution of Turkey: a plate tectonic approach. Tectonophysics, 75, 181–241.
- Şengör, A.M.C., Görür, N. & Şaroğlu, F. (1985). Strike-slip faulting and related basin formation in zones of tectonic escape: Turkey as a case study. In: Biddle, K., Christie-Blick, N. (eds) Strike-Slip Deformation, Basin Formation and Sedimentation. Society of Economic Paleontologists and Mineralogists, 37, 227–264.
- Şengör, A. M. C. (1987). Cross-faults and differential stretching of hanging walls in regions of low-angle normal faulting: examples from western Turkey. Geological Society, London, Special Publications, 28(1), 575-589.
- Seyitoğlu, G., Çemen, İ. & Tekeli, O. (2000). Extensional folding in the Alaşehir (Gediz) Graben, western Turkey. Journal of the Geological Society London, 157, 1097–1100.
- Seyitoğlu, G., Tekeli, O., Çemen, İ., Şen, Ş. & Işık, V. (2002). The role of the flexural rotation/rolling hinge modeling the tectonic evolution of the Alaşehir graben, Western Turkey. Geological Magazine, 139, 15–26.
- Seyitoğlu, G., Işık, V. & Çemen, I. (2004). Complete tertiary exhumation history of the Menderes Massif, Western Turkey: an alternative working hypothesis. Terra Nova, 16, 358–363.
- SÖZBİLİR, H. (2001). Extensional tectonics and the geometry of related macroscopic structures: field evidence from the Gediz detachment, western Turkey. Turkish Journal of Earth Sciences, 10(2), 51-67.
- Sözbilir, H. (2002). Geometry and origin of folding in the Neogene sediments of the Gediz Graben, Western Anatolia, Turkey. Geodinamica Acta, 15, 277–288.
- Sözbilir, H., İnci, U., Erkül, F., Sümer, Ö. (2003). An active intermittent transfer zone accommmodating N-S extension in western Anatolia and its relation to the North Anatolian Fault System. International Workshop on the North Anatolian, East Anatolian and Dead Sea Fault Systems: Recent Progress in Tectonics and Palaeoseismology and Field Training Course in Palaeoseismology, Ankara, Abstracts, 87.
- Sözbilir, H., Sarı, B., Uzel, B., Sümer, Ö., & Akkiraz, S. (2011). Tectonic implications of transtensional supradetachment basin development in an extension-

parallel transfer zone: the Kocaçay Basin, western Anatolia, Turkey. Basin Research, 23(4), 423-448.

- Sperner, B., Ratschbacher, L., & Ott, R. (1993). Fault-striae analysis: a Turbo Pascal program package for graphical presentation and reduced stress tensor calculation. Computers & Geosciences, 19(9), 1361-1388.
- Tauxe, L., & Watson, G. S. (1994). The fold test: an eigen analysis approach. Earth and Planetary Science Letters, 122(3), 331-341.
- Tauxe, L. (2010). Essentials of paleomagnetism. Univ. of California Press. ISO 6
- Taymaz, T., Yilmaz, Y., & Dilek, Y. (2007). The geodynamics of the Aegean and Anatolia: introduction. Geological Society, London, Special Publications, 291(1), 1-16.
- Thébault, E., Finlay, C. C., Beggan, C. D., Alken, P., Aubert, J., Barrois, O., ... & Canet, E. (2015). International geomagnetic reference field: the 12th generation. Earth, Planets and Space, 67(1), 1-19.
- Till, A. B., Roeske, S. M., Bradley, D. C., Friedman, R., & Layer, P. W. (2007). Early Tertiary transtension-related deformation and magmatism along the Tintina fault system, Alaska. Geological Society of America Special Papers, 434, 233-264.
- Uzel, B., & Sözbilir, H. (2008). A first record of a strike-slip basin in western Anatolia and its tectonic implication: the Cumaovası Basin. Turkish Journal of Earth Sciences, 17(3), 559-591.
- Uzel, B., SÖZBİLİR, H., & ÖZKAYMAK, Ç. (2012). Neotectonic evolution of an actively growing superimposed basin in western Anatolia: the inner bay of İzmir, Turkey. Turkish Journal of Earth Sciences, 21(4), 439-471.
- Uzel, B., Sözbilir, H., Özkaymak, Ç., Kaymakcı, N., & Langereis, C. G. (2013). Structural evidence for strike-slip deformation in the Izmir–Balıkesir transfer zone and consequences for late Cenozoic evolution of western Anatolia (Turkey). Journal of Geodynamics, 65, 94-116.
- Uzel, B. (2013). Geologic evolution of the İzmir-Balıkesir Transfer Zone: A crustal-scale structure reorganizing extensional tectonics in western Anatolia (PhD-thesis submitted to Graduate School of Natural and Applied Sciences of Dokuz Eylül University). Dokuz Eylül University, İzmir, Turkey.
- Uzel, B., Langereis, C. G., Kaymakci, N., Sözbilir, H., Özkaymak, Ç., & Özkaptan, M. (2015). Paleomagnetic evidence for an inverse rotation history of Western Anatolia during the exhumation of Menderes core complex. Earth and Planetary Science Letters, 414, 108-125.
- Uzel, B. (2016). Field evidence for normal fault linkage and relay ramp evolution: the Kırkağaç Fault Zone, Western Anatolia (Turkey). Geodinamica Acta, (just-accepted), 1-36. ISO 690
- Uzel, B., Langereis C. G., Kaymakci N., Sözbilir H., Özkaymak, C., Özkaptan, M., İnci, U., Sümer, Ö., Kuiper, K. (2016). Paleomagnetic and geochronologic evidence for a major middle Miocene unconformity in western Anatolia. Journal of the Geological Society.
- Vandenberg, L. C., & Lister, G. S. (1996). Structural analysis of basement tectonites from the Aegean metamorphic core complex of Ios, Cyclades, Greece. Journal of Structural Geology, 18(12), 1437-1454.
- van Hinsbergen, D.J.J., Hafkenscheid, E., Spakman, W., Meulenkamp, J.E. & Wortel, R. (2005b). Nappe stacking resulting from subduction of oceanic and continental lithosphere below Greece. Geology, 33, 325–328.

- van Hinsbergen, D. J. J., Kaymakci, N., Spakman, W., Torsvik, T. H., & Amaru, M. (2010). Reconciling geological history with mantle structure in western Turkey. Earth and Planetary Science Letters, 297, 674-686.
- van Hinsbergen, D. J., Dekkers, M. J., Bozkurt, E., & Koopman, M. (2010). Exhumation with a twist: paleomagnetic constraints on the evolution of the Menderes metamorphic core complex, western Turkey. Tectonics, 29(3).
- Van Velzen, A. J., & Zijderveld, J. D. A. (1992). A method to study alterations of magnetic minerals during thermal demagnetization applied to a fine-grained marine marl (Trubi formation, Sicily). Geophysical Journal International, 110(1), 79-90. ISO 690
- Walcott, C.R., White, S.H. (1998). Constraints on the kinematics of post-orogenic extension imposed by stretching lineations in the Aegean region. Tectonophysics 298, 155– 175.
- Waldron, J.W.F. (2001). Strike-slip systems, lecture notes distributed in Structural Geology and Tectonics EAS 421/521 at University of Alberta.
- Yilmaz, Y., Genç, Ş. C., Gürer, F., Bozcu, M., Yilmaz, K., Karacik, Z., ... & Elmas, A. (2000). When did the western Anatolian grabens begin to develop?. Geological Society, London, Special Publications, 173(1), 353-384.
- Zhu, L., Akyol, N., Mitchell, B.J., Sözbilir, H. (2006). Seismotectonics of western Turkey from high resolution earthquake relocations and moment tensor determinations. Geophysical Research Letters 33, L07316, doi:10.1029/2006GL025842.
- Zijderveld, J.D.A. (1967). AC demagnetization of rocks: analysis of results, in: Collinson, D.W., Creer, K.M. (Eds.), Methods in Paleomagnetism. Elsevier, Amsterdam, pp. 254–286.

# Appendix 1: Tables

### Table 1: Compiled radiometric data for volcanic rocks in the Soma basin

| Locality | Rock type | Age | Source |
|---|---|---|---|
| **Adilköy** | Basalt | 20.40 ± 0.18 | Ersoy et al., 2014 |
| | Basalt | 20.72 ± 0.10 | Ersoy et al., 2014 |
| **Akhisar** | UK-latite | 16.90 ± 0.30 | Ercan et al., 1996 |
| | UK-latite | 16.72 ± 0.15 | Innocenti et al., 2005 |
| **Dededağ** | Andesite | 20.08 ± 0.12 | Ersoy et al., 2014 |
| **Göçbeyli** | Trachyte | 19.77 ± 0.03 | Ersoy et al., 2014 |
| **Sındırgı volcanics** | Rhyolite | 20.20 ± 0.50 | Erkül et al., 2005 |
| | Dacite | 20.30 ± 0.30 | Erkül et al., 2005 |
| **Yuntdağ** | Dacite | 18.76 ± 0.05 | Ersoy et al., 2014 |
| | Andesite | 20.42 ± 0.12 | Ersoy et al., 2014 |
| | Andesite | 17.00 ± 0.30 | Ercan et al., 1996 |

### Table 2: Fault data D1

| Fault plane | | Slip line | | Notes |
|---|---|---|---|---|
| **Strike** | **Dip+dip dir.** | **Azimuth** | **Plunge** | |
| 036 | 82S | 212 | 28 | |
| 018 | 81S | 194 | 22 | |
| 028 | 82S | 198 | 50 | |
| 008 | 81S | 184 | 22 | |
| 032 | 75S | 207 | 17 | |
| 042 | 64N | 226 | 07 | |
| 051 | 65N | 042 | 18 | |
| 043 | 71N | 230 | 21 | |
| 061 | 72N | 250 | 27 | |
| 018 | 57S | 182 | 23 | |
| 016 | 77S | 191 | 22 | |
| 044 | 68S | 055 | 25 | |

### Table 3: Fault data S1

| Fault plane | | Slip line | | Notes |
|---|---|---|---|---|
| **Strike** | **Dip+dip dir.** | **Azimuth** | **Plunge** | |
| 122 | 75S | 161 | 67 | |
| 098 | 85S | 105 | 53 | |
| 082 | 82S | 095 | 57 | |
| 139 | 72S | 146 | 21 | |
| 114 | 89S | 117 | 73 | |
| 143 | 70S | 182 | 60 | |

## Table 4: Fault data N1

| Fault plane | | Slip line | | Notes |
|---|---|---|---|---|
| **Strike** | **Dip+dip dir.** | **Azimuth** | **Plunge** | |
| 161 | 42E | 076 | 42 | Kirkağaç fault |
| 099 | 60N | 026 | 60 | Bakır fault |
| 070 | 78E | 123 | 75 | |
| 122 | 75S | 161 | 67 | |
| 102 | 67S | 214 | 65 | |
| 083 | 65S | 239 | 42 | |
| 098 | 85S | 105 | 53 | |
| 082 | 82S | 095 | 57 | |
| 108 | 70N | 075 | 56 | |
| 062 | 55N | 015 | 46 | |
| 057 | 78N | 019 | 71 | |
| 064 | 79N | 024 | 73 | |
| 049 | 68N | 003 | 61 | |
| 038 | 71N | 347 | 66 | |
| 081 | 61N | 015 | 59 | |
| 096 | 61N | 040 | 56 | |
| 080 | 83S | 255 | 35 | |
| 114 | 89S | 117 | 73 | |
| 105 | 72S | 268 | 42 | |
| 143 | 70S | 182 | 60 | |
| 129 | 62S | 181 | 56 | |
| 125 | 78S | 278 | 65 | |
| 115 | 65S | 237 | 61 | |
| 095 | 78S | 122 | 65 | |
| 161 | 42E | 076 | 42 | |
| 099 | 60N | 026 | 60 | |
| 070 | 78E | 123 | 75 | |
| 122 | 75S | 161 | 67 | |
| 102 | 67S | 214 | 65 | |
| 083 | 65S | 239 | 42 | |
| 098 | 85S | 105 | 53 | |
| 082 | 82S | 095 | 57 | |
| 108 | 70N | 075 | 56 | |
| 062 | 55N | 015 | 46 | |
| 057 | 78N | 019 | 71 | |
| 064 | 79N | 024 | 73 | |
| 049 | 68N | 003 | 61 | |
| 038 | 71N | 347 | 66 | |
| 081 | 61N | 015 | 59 | |
| 096 | 61N | 040 | 56 | |
| 080 | 83S | 255 | 35 | |
| 114 | 89S | 117 | 73 | |
| 105 | 72S | 268 | 42 | |
| 143 | 70S | 182 | 60 | |
| 129 | 62S | 181 | 56 | |
| 125 | 78S | 278 | 65 | |
| 115 | 65S | 237 | 61 | |
| 95 | 78S | 122 | 65 | |

## Table 5: Paleomagnetic results

*Paleomagnetic data from every measured site and locality from this study in both a geographic and tectonic reference frame. Legend: Name = Locality/site name (Volcanic sites are indicated with a *, sedimentary sites do not have an annotation. Rejected sites are listed in cursive. The most reliable reference frame for every locality is listed in brackets behind the locality name with tc = tectonic correction, no tc = no tectonic correction); N = number of samples/sites used for the mean after a fixed cut-off (45°); D = mean declination; I = mean inclination; k = dispersion of directions; α95 = Fisher cone of confidence (directions); K = dispersion of virtual geomagnetic poles (VGPs); $\Delta D_x$ = corresponding error in declination (Butler, 1992); A95 = Fisher cone of confidence (VGP's); $A95_{min}$ and $A95_{max}$ = confidence envelope of Deenen et al. (2011, 2014); Tilt = azimuth/dip of bedding used for tectonic correction.*

| **Name** | **N** | **Geographic (no tc)** | | | | | | | **Tilt** | **Tectonic (tc)** | | | | | | |
|---|---|---|---|---|---|---|---|---|---|---|---|---|---|---|---|---|
| | | **D** | **I** | **k** | **α95** | **K** | **$\Delta D_x$** | **$A95_{min}$<A95<$A95_{max}$** | | **D** | **I** | **k** | **α95** | **K** | **$\Delta D_x$** | **$A95_{min}$<A95<$A95_{max}$** |
| **AD (no tc)** | | | | | | | | | | | | | | | | |
| AD01* | 7 | 196.4 | -36.3 | 361.6 | 3.2 | 320.1 | 3.6 | 3.4<5.5=$A95_{min}$ | 278/44 | 195.8 | 7.4 | 361.6 | 3.2 | 459.0 | 2.8 | 2.8<5.5=$A95_{min}$ |
| *AD02** | *6* | *89.7* | *-48.3* | 282.4 | *4.0* | *250.6* | *4.9* | *4.2<5.9=$A95_{min}$* | *153/50* | *80.4* | *-1.4* | *282.4* | *4.0* | *592.9* | *2.8* | *2.8<5.9=$A95_{min}$* |
| AD03* | 4 | 210.3 | -48.3 | 36.3 | 15.5 | 26.5 | 21.0 | 6.9<18.2<34.2 | 153/50 | 122.3 | -65.4 | 36.3 | 15.5 | 18.5 | 33.5 | 6.9<21.9<34.2 |
| AD04* | 3 | 217.7 | -41.6 | 1898.3 | 2.8 | 1898.3 | 3.7 | 3.4<7.7=$A95_{min}$ | 203/45 | 178.2 | -37.1 | 1898.3 | 2.8 | 2240.4 | 2.8 | 2.6<7.7=$A95_{min}$ |
| AD05* | 3 | 202.8 | -48.1 | 407.4 | 6.1 | 509.0 | 6.3 | 5.5<7.7=$A95_{min}$ | 203/45 | 164.7 | -31.6 | 407.4 | 6.1 | 361.4 | 6.8 | 6.5<7.7=$A95_{min}$ |
| AD06* | 4 | 201.9 | -49.0 | 52.5 | 12.8 | 38.5 | 17.4 | 6.9<15.0<34.2 | 203/45 | 163.4 | -31.7 | 52.5 | 12.8 | 75.2 | 11.2 | 6.9<10.7<34.2 |
| AD07* | 6 | 192.6 | -59.1 | 33.0 | 11.8 | 17.4 | 21.7 | 5.9<16.5<26.5 | 203/45 | 149.9 | -32.8 | 33.0 | 11.8 | 38.2 | 11.5 | 5.9<11.0<26.5 |
| | **6** | **204.1** | **-47.4** | **67.2** | **8.2** | **60.7** | **9.9** | **5.9<8.7<26.5** | | **166.9** | **-33.7** | **7.8** | **25.5** | **9.2** | **24.7** | **5.9<23.4<26.5** |
| **BG (tc)** | | | | | | | | | | | | | | | | |
| BG01* | 4 | 339.9 | 59.4 | 86.2 | 10.0 | 42.3 | 18.9 | 6.9<14.3<34.2 | 055/18 | 357.9 | 76.1 | 86.2 | 10.0 | 26.4 | 44.9 | 6.9<18.2<34.2 |
| *BG02** | *4* | *105.8* | *-33.7* | *167.7* | *7.1* | *228.6* | *6.4* | *6.1<6.9=*$A95_{min}$ | *055/18* | *105.8* | *-33.7* | *167.7* | *7.1* | *228.6* | *6.4* | *6.1<6.9=* $A95_{min}$ |
| BG03* | 4 | 338.8 | 55.7 | 42.4 | 14.3 | 28.0 | 22.1 | 6.9<17.7<34.2 | 055/18 | 351.8 | 72.8 | 42.4 | 14.3 | 15.8 | 50.1 | 6.9<23.9<34.2 |
| | **2** | **339.3** | **57.6** | **947.1** | **8.1** | **803.0** | **11.3** | **8.8<9.1=A95min** | | **354.6** | **74.5** | **947.1** | **8.1** | **336.6** | **29.0** | **9.1<13.7<53.0** |
| ***BO*** | - | - | - | - | - | - | - | - | | - | - | - | - | - | - | - |
| **BY (tc)** | | | | | | | | | | | | | | | | |
| BY01* | 4 | 26.2 | 61.4 | 19.3 | 21.4 | 13.5 | 36.5 | 6.9<26.0<34.2 | 245/15 | 10.8 | 50.4 | 19.3 | 21.4 | 15.6 | 28.4 | 6.9<24.0<34.2 |
| BY02* | 3 | 337.7 | 66.7 | 84.3 | 13.5 | 37.4 | 32.3 | 7.7<20.4<41.0 | 245/15 | 336.7 | 51.7 | 84.3 | 13.5 | 64.9 | 18.4 | 7.7<15.4<41.0 |
| BY03* | 4 | 330.9 | 71.3 | 53.2 | 12.7 | 21.0 | 38.7 | 6.9<20.5<34.2 | *245/15* | 332.7 | 56.3 | 53.2 | 12.7 | 34.1 | 20.1 | 6.9<16.0<34.2 |
| BY04* | 3 | 41.3 | 59.0 | 16.8 | 31.1 | 12.4 | 50.8 | 7.7<36.5<41.0 | 245/14 | 23.1 | 50.7 | 16.8 | 31.1 | 18.5 | 35.3 | 7.7<29.5<41.0 |
| BY05* | 3 | 61.2 | 62.9 | 251.7 | 7.8 | 130.0 | 15.3 | 7.7<10.9<41.0 | 245/14 | 35.3 | 58.4 | 251.7 | 7.8 | 121.8 | 14.5 | 7.7<11.2<41.0 |
| *BY06** | *3* | *294.9* | *21.1* | *5.7* | *57.1* | *8.3* | *47.1* | $A95_{max}$=41.0<46.0 | *145/14* | *291.1* | *13.7* | *5.7* | *57.1* | *8.5* | *45.7* | *$A95_{max}$=41.0<45.7* |
| | **5** | **20.9** | **68.1** | **24.8** | **15.7** | **9.6** | **44.5** | **6.3<26.0<29.7** | | **3.6** | **56.0** | **24.8** | **15.7** | **12.7** | **28.2** | **6.3<22.3<29.7** |
| **DK (tc)** | | | | | | | | | | | | | | | | |
| DK01 | 10 | 0.6 | 54.7 | 43.9 | 7.4 | 35.4 | 10.1 | 4.8<8.2<19.2 | 018/29 | 41.9 | 52.9 | 43.9 | 7.4 | 39.4 | 9.3 | 4.8<7.8<19.2 |
| | **10** | **0.6** | **54.7** | **43.9** | **7.4** | **35.4** | **10.1** | **4.8<8.2<19.2** | | **41.9** | **52.9** | **43.9** | **7.4** | **39.4** | **9.3** | **4.8<7.8<19.2** |
| **EV (tc)** | | | | | | | | | | | | | | | | |
| EV01 | 5 | 253.5 | -19.6 | 21.1 | 17.1 | 27.8 | 15.0 | 6.3<14.8<29.7 | 160/20 | 254.3 | -39.5 | 21.1 | 17.1 | 20.3 | 18.9 | 6.3<17.4<29.7 |
| EV02 | 5 | 58.0 | 34.0 | 40.3 | 12.2 | 75.3 | 13.6 | 6.3<8.9<29.7 | 160/20 | 53.1 | 53.4 | 40.3 | 12.2 | 38.6 | 15.1 | 6.3<12.5<29.7 |
| EV03 | 5 | 53.3 | 21.5 | 94.1 | 7.9 | 292.8 | 4.6 | 4.5<6.3=$A95_{min}$ | 160/20 | 49.4 | 40.4 | 94.1 | 7.9 | 164.3 | 6.5 | 6.0<6.3=$A95_{min}$ |
| EV04 | 5 | 243.4 | -34.1 | 66.7 | 9.4 | 61.7 | 10.4 | 6.3<9.8<29.7 | 160/20 | 240.8 | -53.9 | 66.7 | 39.2 | 39.2 | 15.1 | 6.3<12.4<29.7 |
| | **20** | **62.1** | **27.5** | **28.5** | **6.2** | **38.4** | **5.5** | **3.6<5.3<12.4** | | **59.6** | **47.3** | **28.5** | **6.2** | **24.8** | **7.6** | **3.6<6.7<12.4** |
| **GB (no tc)** | | | | | | | | | | | | | | | | |
| GB01* | 8 | 191.0 | -40.2 | 72.0 | 6.6 | 69.4 | 7.3 | 5.2<6.7<22.1 | 135/40 | 144.4 | -64.3 | 72.0 | 6.6 | 35.9 | 13.6 | 5.2<9.4<22.1 |
| GB02* | 6 | 183.2 | -23.2 | 215.3 | 4.6 | 348.3 | 3.7 | 3.6<5.9=$A95_{min}$ | 265/20 | 182.5 | -3.4 | 215.3 | 4.6 | 403.4 | 3.3 | 3.3<5.9=$A95_{min}$ |
| GB03* | 7 | 195.9 | -9.7 | 203.7 | 4.2 | 242.5 | 3.9 | 3.9<5.5=$A95_{min}$ | 265/20 | 195.8 | 9.0 | 203.7 | 4.2 | 242.8 | 3.9 | 3.9<5.5=$A95_{min}$ |
| GB04* | 5 | 196.6 | -32.5 | 130.3 | 6.7 | 278.2 | 4.8 | 4.6<6.3=$A95_{min}$ | 265/20 | 193.6 | -13.7 | 130.3 | 6.7 | 415.1 | 3.8 | 3.8<6.3=$A95_{min}$ |
| *GB05** | *6* | *248.5* | *17.8* | *3.5* | *41.7* | *5.5* | *31.7* | *$A95_{max}$=26.5<31.3* | *265/20* | *266.6* | *27.9* | *4.2* | *42.2* | *5.6* | *36.9* | *$A95_{max}$=29.7<35.5* |
| *GB06** | *4* | *113.2* | *37.3* | *5.8* | *41.9* | *6.2* | *43.4* | *$A95_{max}$=34.2<40.0* | *265/20* | *96.7* | *44.3* | *5.8* | *41.9* | *5.3* | *50.6* | *$A95_{max}$=34.2<44.0* |
| GB07* | 5 | 212.9 | -0.2 | 16.3 | 19.5 | 26.4 | 15.2 | 6.3<15.2<29.7 | 265/22 | 215.0 | 16.9 | 16.3 | 19.5 | 27.9 | 14.9 | 6.3<14.7<29.7 |
| GB08* | 7 | 208.5 | -67.3 | 413.7 | 3.0 | 170.1 | 7.2 | 4.6<5.5=$A95_{min}$ | 265/22 | 193.3 | -47.3 | 413.7 | 3.0 | 313.1 | 3.9 | 3.4<5.5=$A95_{min}$ |
| GB09* | 7 | 190.1 | -26.6 | 296.7 | 3.5 | 336.2 | 3.4 | 3.3<5.5=$A95_{min}$ | 265/22 | 188.5 | -5.3 | 296.7 | 3.5 | 462.7 | 2.8 | 2.8<5.5=$A95_{min}$ |
| | **7** | **196.2** | **-28.7** | **12.2** | **18.0** | **18.5** | **15.0** | **5.5<14.4<24.1** | | **194.7** | **-7.0** | **10.9** | **21.2** | **23.0** | **14.3** | **5.9<14.3<26.5** |
| **GL (no tc)** | | | | | | | | | | | | | | | | |
| GL01* | 3 | 47.6 | 43.8 | 251.9 | 7.8 | 236.6 | 8.9 | 7.7<8.0<41.0 | 000/00 | 47.6 | 43.8 | 251.9 | 7.8 | 236.6 | 8.9 | 7.7<8.0<41.0 |
| GL02* | 5 | 228.8 | -4.1 | 67.6 | 9.4 | 74.7 | 8.9 | 6.3<8.9<29.7 | 000/00 | 228.8 | -4.1 | 67.6 | 9.4 | 74.7 | 8.9 | 6.3<8.9<29.7 |
| GL03* | 3 | 194.0 | -58.5 | 3741.3 | 2.0 | 1828.9 | 3.7 | 2.9<7.7=$A95_{min}$ | 000/00 | 194.0 | -58.5 | 3741.3 | 2.0 | 1828.9 | 3.7 | 2.9<7.7=$A95_{min}$ |
| GL04* | 3 | 151.1 | -50.1 | 40.5 | 19.6 | 29.9 | 27.0 | 7.7<22.9<41.0 | 000/00 | 151.1 | -50.1 | 40.5 | 19.6 | 29.9 | 27.0 | 7.7<22.9<41.0 |

| | | | | | | | | | | | | | | | | |
|---|---|---|---|---|---|---|---|---|---|---|---|---|---|---|---|---|
| GL05* | 5 | 192.1 | -26.6 | 60.2 | 9.9 | 72.9 | 9.3 | 6.3<9.0<29.7 | 000/00 | 192.1 | -26.6 | 60.2 | 9.9 | 72.9 | 9.3 | 6.3<9.0<29.7 |
| GL06* | 2 | 166.6 | -66.7 | 73.5 | 29.6 | 35.8 | NaN | 9.1<43.0<53.0 | 065/19 | 204.6 | -84.0 | 73.5 | 29.5 | 19.6 | NaN | $A95_{max}$=53.0<59.8 |
| | **6** | **19.0** | **45.6** | **6.7** | **28.0** | **6.5** | **32.4** | **$A95_{max}$=26.5<28.5** | | **22.7** | **48.0** | **5.9** | **30.1** | **5.3** | **37.7** | **$A95_{max}$=26.5<32.3** |
| **HM (no tc)** | | | | | | | | | | | | | | | | |
| HM01* | 6 | 320.5 | 63.8 | 54.3 | 9.2 | 32.1 | 17.2 | 5.9<12.0<26.5 | 290/25 | 346.8 | 45.9 | 54.3 | 9.2 | 56.0 | 10.2 | 5.9<9.0<26.5 |
| HM02* | 3 | 353.0 | 64.5 | 24.8 | 25.3 | 11.7 | 62.5 | 7.7<37.7<41.0 | 290/25 | 5.0 | 41.0 | 24.8 | 25.3 | 18.8 | 32.2 | 7.7<29.3<41.0 |
| HM03 | 7 | 152.2 | -58.2 | 33.4 | 10.6 | 20.7 | 17.5 | 5.5<13.6<24.1 | 171/16 | 132.5 | -50.3 | 33.4 | 10.6 | 28.7 | 13.4 | 5.5<11.5<24.1 |
| HM04* | 3 | 349.5 | 20.7 | 10.0 | 41.2 | 14.2 | 34.6 | 7.7<34.0<41.0 | 280/04 | 350.0 | 16.9 | 10.0 | 41.2 | 14.9 | 33.6 | 7.7<33.1<41.0 |
| HM05* | 6 | 357.3 | 31.2 | 131.3 | 5.9 | 180.0 | 5.2 | 5.0<5.9=$A95_{min}$ | 090/32 | 355.0 | 63.2 | 131.3 | 5.9 | 69.5 | 11.4 | 5.9<8.1<26.5 |
| *HM06** | *2* | *165.3* | *25.7* | *29.6* | *47.6* | *84.0* | *28.5* | *9.1<27.6<53.0* | *090/32* | *166.7* | *-5.4* | *29.6* | *47.6* | *113.8* | *23.7* | *9.1<23.6<53.0* |
| | **11** | **338.3** | **54.0** | **18.5** | **10.9** | **16.6** | **14.1** | **4.6<11.6<18.1** | | **328.7** | **49.2** | **14.7** | **12.3** | **12.3** | **15.7** | **4.6<13.6<18.1** |
| **IL (no tc)** | | | | | | | | | | | | | | | | |
| IL01 | 5 | 11.1 | 48.3 | 78.6 | 8.7 | 55.5 | 11.9 | 6.3<10.4<29.7 | 119/24 | 352.3 | 70.0 | 78.6 | 8.7 | 30.2 | 24.5 | 6.3<14.2<29.7 |
| *IL02* | *3* | *118.7* | *24.5* | *21.3* | *27.4* | *20.0* | *29.1* | *7.7<28.3<41.0* | *080/28* | *124.5* | *5.6* | *21.3* | *27.4* | *28.0* | *23.8* | *7.7<23.8<41.0* |
| IL03 | 4 | 15.3 | 44.2 | 15.3 | 44.2 | 378.0 | 5.3 | 4.7<6.9=$A95_{min}$ | 100/08 | 16.2 | 52.1 | 384.9 | 4.7 | 297.6 | 6.3 | 5.3<6.9=$A95_{min}$ |
| IL04 | 5 | 22.0 | 37.4 | 94.1 | 7.9 | 85.4 | 8.9 | 6.3<8.3<29.7 | 130/22 | 12.6 | 57.8 | 94.1 | 7.9 | 50.0 | 14.0 | 6.3<10.9<29.7 |
| IL05 | 4 | 41.2 | 40.9 | 75.5 | 10.6 | 91.3 | 10.5 | 6.9<9.7<34.2 | 160/12 | 34.6 | 51.0 | 75.5 | 10.6 | 67.7 | 13.3 | 6.9<11.2<34.2 |
| IL06 | 4 | 31.3 | 41.9 | 10.5 | 29.8 | 9.7 | 34.5 | 6.9<31.1<34.2 | 149/12 | 24.6 | 52.2 | 10.5 | 29.8 | 7.3 | 45.1 | $A95_{max}$=34.2<36.5 |
| IL07 | 2 | 210.8 | -29.5 | 805.6 | 8.8 | 1073.4 | 7.9 | 7.6<9.1=$A95_{min}$ | 023/15 | 218.7 | -26.5 | 805.6 | 8.8 | 850.6 | 8.8 | 8.6<9.1=$A95_{min}$ |
| IL08 | 3 | 54.1 | 42.5 | 7.4 | 48.8 | 5.7 | 67.9 | 7.7-41.0-67.9 | 235/23 | 34.6 | 38.1 | 7.4 | 48.8 | 7.6 | 53.0 | $A95_{max}$=41.0<48.1 |
| | **27** | **25.4** | **41.5** | **30.3** | **5.2** | **26.2** | **6.2** | **3.3<5.6<10.5** | | **21.4** | **52.8** | **18.5** | **6.8** | **15.1** | **9.1** | **3.3<7.6<10.5** |
| **KD (no tc)** | | | | | | | | | | | | | | | | |
| KD01* | 8 | 204.6 | -46.7 | 196.2 | 4.0 | 170.2 | 4.8 | 4.3<5.2=$A95_{min}$ | 327/15 | 210.8 | -33.6 | 196.2 | 4.0 | 241.0 | 3.8 | 3.6<5.2=$A95_{min}$ |
| KD02* | 7 | 207.0 | -48.5 | 39.7 | 9.7 | 24.3 | 14.4 | 5.5<12.5<24.1 | 021/15 | 22.6 | -44.9 | 39.7 | 9.7 | 28.5 | 12.9 | 5.5<11.5<24.1 |
| KD03* | 7 | 214.6 | -6.7 | 214.6 | -6.7 | 97.7 | 6.1 | 5.5<6.1<24.1 | 103/22 | 217.2 | -27.0 | 53.9 | 8.3 | 94.2 | 6.5 | 5.5<6.3<24.1 |
| KD04* | 7 | 210.7 | -47.7 | 133.6 | 5.2 | 85.9 | 7.5 | 5.5<6.5<24.1 | 062/16 | 229.1 | -53.9 | 133.6 | 5.2 | 74.4 | 8.5 | 5.5<7.0<24.1 |
| KD05* | 7 | 214.7 | -48.7 | 77.0 | 6.9 | 45.7 | 10.4 | 5.5<9.0<24.1 | 062/16 | 233.8 | -53.7 | 77.0 | 6.9 | 42.9 | 11.3 | 5.5<9.3<24.1 |
| KD06* | 6 | 205.0 | -50.3 | 239.5 | 4.3 | 187.4 | 5.7 | 4.9<5.9=$A95_{min}$ | 075/15 | 221.3 | -60.4 | 239.5 | 4.3 | 113.8 | 8.4 | 5.9<6.3<26.5 |
| KD07* | 7 | 212.2 | -47.2 | 203.7 | 4.2 | 158.1 | 5.5 | 4.8<5.5=$A95_{min}$ | 075/15 | 227.8 | -55.9 | 203.7 | 4.2 | 124.5 | 6.8 | 5.4<5.5=$A95_{min}$ |
| | **7** | **210.1** | **-42.7** | **26.2** | **12.0** | **59.4** | **8.7** | **5.5<7.9<24.1** | | **222.2** | **-47.3** | **35.7** | **10.2** | **44.9** | **10.4** | **5.5<9.1<24.1** |
| **KG (tc)** | | | | | | | | | | | | | | | | |
| KG01 | 5 | 355.8 | 50.5 | 54.4 | 10.5 | 48.7 | 13.0 | 6.3<11.1<29.7 | 120/20 | 332.9 | 64.8 | 54.4 | 10.5 | 29.8 | 21.0 | 6.3<14.2<29.7 |
| | **5** | **355.8** | **50.5** | **54.4** | **10.5** | **48.7** | **13.0** | **6.3<11.1<29.7** | | **332.9** | **64.8** | **54.4** | **10.5** | **29.8** | **21.0** | **6.3-14.2-29.7** |
| **KN (tc)** | | | | | | | | | | | | | | | | |
| KN01 | 4 | 190.6 | -62.6 | 97.8 | 9.3 | 40.8 | 20.4 | 6.9<14.6<34.2 | 034/20 | 231.3 | -63.7 | 97.8 | 9.3 | 46.9 | 19.5 | 6.9<13.5<34.2 |
| *KN02* | *3* | *222.0* | *11.4* | *2.9* | *93.0* | *4.6* | *66.4* | *$A95_{max}$=41.0<65.8* | *347/19* | *218.1* | *26.7* | *2.9* | *93.0* | *3.9* | *82.0* | *$A95_{max}$=41.0<73.8* |
| *KN03* | *2* | *154.5* | *6.8* | *4.7* | *NaN* | *13.5* | *74.9* | *$A95_{max}$=53.0<74.5* | *335/21* | *152.1* | *6.2* | *4.7* | *NaN* | *8.3* | *77.5* | *$A95_{max}$=53.0<103* |
| *KN04* | *1* | *345.0* | *39.2* | *NaN* | *NaN* | *NaN* | *NaN* | *12.0< NaN<82.0* | *060/24* | *355.1* | *61.8* | *NaN* | *NaN* | *NaN* | *NaN* | *12.0< NaN<82.0* |
| | **4** | **190.6** | **-62.6** | **97.8** | **9.3** | **40.8** | **20.4** | **6.9<14.6<34.2** | | **231.3** | **-63.7** | **97.8** | **9.3** | **46.9** | **19.5** | **6.9<13.5<34.2** |
| ***KP*** | - | - | - | - | - | - | - | - | | - | - | - | - | - | - | - |
| **SV (no tc)** | | | | | | | | | | | | | | | | |
| SV01 | 4 | 2.8 | 35.2 | 4.3 | 50.2 | 6.3 | 42.8 | $A95_{max}$=34.2<39.8 | 001/64 | 34.0 | 13.3 | 4.3 | 50.2 | 5.8 | 42.3 | $A95_{max}$=34.2<41.9 |
| SV02 | 10 | 34.3 | 35.3 | 12.3 | 14.4 | 12.1 | 15.4 | 4.8<14.5<19.2 | 229/24 | 16.8 | 22.9 | 8.7 | 16.5 | 12.0 | 14.0 | 4.6<13.7<18.1 |
| | **14** | **28.3** | **41.1** | **10.4** | **12.9** | **10.1** | **14.4** | **4.2<13.2<15.6** | | **19.1** | **24.8** | **7.6** | **14.3** | **9.5** | **13.0** | **4.0<12.7<14.3** |

## Table 6: Block mean paleomagnetic results

*Block mean paleomagnetic results from this study (1) and revisited data of (2) Uzel et al. (2015) and (3) van Hinsbergen et al. (2010). Legend: N = number of samples/sites used for the mean after a fixed cut-off (45°); D = mean declination; I = mean inclination; k = dispersion of directions; α95 = Fisher cone of confidence (directions); K = dispersion of virtual geomagnetic poles (VGPs); $\Delta D_x$ = corresponding error in declination (Butler, 1992); A95 = Fisher cone of confidence (VGP's); $A95_{min}$ and $A95_{max}$ = confidence envelope of Deenen et al. (2011, 2014).*

| **Locality** | **N** | **D** | **I** | **k** | **α95** | **K** | **$\Delta D_x$** | **$A95_{min}$<A95<$A95_{max}$** |
|---|---|---|---|---|---|---|---|---|
| **Bakır (1)** | | | | | | | | |
| Gelenbe (GL) | 6 | 19.0 | 45.6 | 6.7 | 28.0 | 6.5 | 32.4 | $A95_{max}$=26.5<28.5 |
| İlyaslar (IL) | 27 | 25.4 | 41.5 | 30.3 | 5.2 | 26.2 | 6.2 | 3.3<5.6<10.5 |
| Selvili (SV) | 14 | 28.3 | 41.1 | 10.4 | 12.9 | 10.1 | 14.4 | 4.2<13.2<15.6 |
| | **47** | **26.5** | **41.5** | **16.6** | **5.4** | **15.8** | **6.0** | **2.6<5.5<7.5** |
| **Kınık (1)** | | | | | | | | |
| Arpadere (AD) | 6 | 204.1 | -47.4 | 67.2 | 8.2 | 60.7 | 9.9 | 5.9<8.7<26.5 |
| Bağalan (BG) | 2 | 354.6 | 74.5 | 947.1 | 8.1 | 336.6 | 29.0 | 9.1<13.7<53.0 |
| Dereköy (DK) | 10 | 41.9 | 52.9 | 43.9 | 7.4 | 39.4 | 9.3 | 4.8<7.8<19.2 |
| Karadere (KD) | 7 | 210.1 | -42.7 | 26.2 | 12.0 | 59.4 | 8.7 | 5.5<7.9<24.1 |
| Kınık (KN) | 4 | 231.3 | -63.7 | 97.8 | 9.3 | 46.9 | 19.5 | 6.9<13.5<34.2 |
| | **29** | **33.9** | **52.8** | **25.8** | **5.4** | **21.6** | **7.1** | **3.1<5.9<9.8** |
| **Ahmetlar (3)** | **5** | **-** | **-** | **-** | **-** | **-** | **-** | **-** |
| **Demirci (3)** | **10** | **34.7** | **49.0** | **11.3** | **15.0** | **8.8** | **20.0** | **4.8<17.2<19.2** |
| **Gördes (2,3)** | **31** | **335.5** | **53.0** | **24.0** | **5.4** | **17.6** | **7.6** | **3.0<6.3<9.4** |
| **Güre (3)** | **4** | **17.7** | **51.8** | **61.4** | **11.8** | **46.2** | **16.2** | **6.9<13.7<34.2** |
| **Selendi (3)** | **19** | **7.2** | **53.8** | **37.1** | **5.6** | **33.2** | **7.2** | **3.7<5.9<12.8** |
| **Uşak (3)** | **3** | **343.4** | **54.9** | **20.8** | **27.7** | **13.6** | **44.4** | **7.7<34.8<41.0** |